



6/24/67

OFFICE OF NAS  
100-10113

# TECHNICAL MEMORANDUM

DECLASSIFIED-AUTHORITY-MEMO.US:  
X-6292313. TAINE TO SIRUKLAS  
DATED JUNE 15, 1967

## FLIGHT TEST OF A LITTLE JOE BOOSTED FULL-SCALE SPACECRAFT MODEL AND ESCAPE SYSTEM FOR PROJECT MERCURY

By Hal T. Baber, Jr., Howard S. Carter,  
and Roland D. English

Langley Research Center  
Langley Station, Hampton, Va.

UNIT PRICE \$ \_\_\_\_\_

UNIT PRICE(S) \$ \_\_\_\_\_

Hard copy (HC) 5.68

Microfiche (MF) 6.5

FACILITY FORM 442

ACCESSION NUMBER

PAGES

NASA CR OR TMX OR AD NUMBER

(THRU)

(CODE)

(CATEGORY)

UNCLASSIFIED

ling the national defense of the United States within the meaning  
secs. 793 and 794, the transmission or revelation of which in any

NATIONAL AERONAUTICS AND SPACE ADMINISTRATION

WASHINGTON

downgraded this year

May 1962

is: declassified

**CONFIDENTIAL**

CONFIDENTIAL

NATIONAL AERONAUTICS AND SPACE ADMINISTRATION

TECHNICAL MEMORANDUM X-629

FLIGHT TEST OF A LITTLE JOE BOOSTED FULL-SCALE SPACECRAFT

MODEL AND ESCAPE SYSTEM FOR PROJECT MERCURY\*

By Hal T. Baber, Jr., Howard S. Carter,  
and Roland D. English

SUMMARY


The third flight test in the Little Joe program was made on December 4, 1959, from NASA Wallops Station as part of the Project Mercury manned-satellite program. This flight test of a full-scale spacecraft model and associated escape system demonstrated the soundness of the escape-system concept at trajectory conditions of low dynamic pressure and hypersonic speed. During atmospheric entry, the maximum angle of attack experienced by the spacecraft was approximately  $100^{\circ}$ ; the drag coefficient was essentially invariant with Mach number at supersonic and hypersonic speeds. Analysis of entry motions of the spacecraft indicated that it was statically stable but dynamically unstable. The biological package onboard the spacecraft functioned as desired and the rhesus monkey housed in the package withstood the forces encountered during the flight with no apparent physical harm. The performance of the recovery aids was satisfactory, with location and recovery of the spacecraft accomplished  $1\frac{3}{4}$  hours from the time of launch.

INTRODUCTION

Orbital flight of a manned spacecraft is the principal aim of Project Mercury. In the conduct of this program, extensive effort is being expended to perfect the spacecraft and associated equipment.

As part of this program, the Langley Research Center has been engaged in a research and development effort directed toward establishment of the feasibility of the escape-system concept, which is to afford

\*Title, Unclassified.



CONFIDENTIAL

safety for the astronaut in the event of mission abort during the atmospheric-ascent phase. Results of a flight test of the escape system which simulated escape from the launch vehicle prior to lift-off are presented in reference 1. After this "beach abort" test demonstrated the satisfactory functioning of the escape system under this condition, it was necessary to demonstrate escape-system capability during boosted flight. In addition, there existed a requirement to determine the aerodynamic forces on the spacecraft during boosted flight and the spacecraft motions during entry.

For the purpose of investigating the aforementioned problems, the Little Joe flight test program came into being. This program, which has been under the direction of the Langley Research Center, employed full-scale models of the Mercury spacecraft propelled by a launch vehicle consisting of a cluster of six or eight solid-propellant rocket motors for one and two propulsion stages, respectively. In the first flight test in the Little Joe program a "boiler plate" spacecraft model with a mock escape system attached was used as a qualification test of the launch vehicle and the destruct system. The results of this flight test, which indicated the adequacy of these systems, are reported in reference 2. The second flight test in this program had as its objective a low-altitude, high-dynamic-pressure proof test of the escape system. The point on the Little Joe trajectory selected for initiation of the abort sequence corresponded to the most severe ascent flight condition anticipated for the Mercury (Atlas boosted) flight.

Results obtained from the third flight test in the Little Joe program are presented herein. The primary purpose of this test was to study the operation of the spacecraft escape system under conditions of low dynamic pressure and high Mach number. In addition, information on aerodynamic loads, aerodynamic heating, and spacecraft motions during entry were obtained. The School of Aviation Medicine, U.S. Air Force, provided a biological package for testing the reactions of a small primate under the influence of high accelerations, weightlessness, and entry motions. The vehicle employed in this test consisted of a two-stage Little Joe launch vehicle, a full-scale model of the Mercury spacecraft more rigorously designed and instrumented than other models in the Little Joe program, and a production escape system.

This flight test, which took place December 4, 1959, was conducted at NASA Wallops Station as were the other flights in the Little Joe program.

CONFIDENTIAL

CONFIDENTIAL

3

# SYMBOLS

In the present paper, distances are measured in the U.S. foot.  
(One U.S. foot = 0.3048006 meter.)

All coefficients are based on 30.27 square feet, the maximum cross-sectional area of the spacecraft.

A	spacecraft cross-sectional area at maximum body diameter, 30.27 sq ft
$a_D$	acceleration along the velocity vector, g units
$a_L$	longitudinal acceleration, g units (fig. 1)
$a_N$	normal acceleration, g units (fig. 1)
$a_R$	resultant of normal and transverse accelerations, g units
$a_T$	transverse acceleration, g units (fig. 1)
$C_A$	axial-force coefficient
$C_D$	drag coefficient
$C_{D,\alpha \approx 0}$	drag coefficient at approximately zero angle of attack
$C_{L\alpha}$	lift-curve slope, 1/radian
$C_{m\alpha}$	pitching-moment-curve slope, 1/deg
$C_{m\dot{q}} + C_{m\ddot{\alpha}}$	damping-in-pitch derivative, 1/radian
$C_N$	normal-force coefficient
$C_R$	resultant-force coefficient
$C_Y$	side-force coefficient
d	maximum diameter of spacecraft, 6.21 ft



CONFIDENTIAL

$g$	unit of acceleration
$I_Y$	pitch moment of inertia, 5,650 slug-ft <sup>2</sup> for spacecraft-tower combination, 503 slug-ft <sup>2</sup> for spacecraft alone
$l$	cone length, ft
$M$	free-stream Mach number
$M_{av}$	average Mach number
$P$	period of oscillatory motion, sec
$p_l$	local surface pressure, lb/sq ft abs
$p_\infty$	free-stream surface pressure, lb/sq ft abs
$q$	free-stream dynamic pressure, lb/sq ft
$X, Y, Z$	coordinate axes for spacecraft (fig. 1)
$\alpha$	angle of attack, deg
$\alpha_{R, max}$	maximum resultant angle of attack, deg
$\dot{\alpha}_{R, max}$	time rate of change of maximum resultant angle of attack, radians/sec
$\dot{\theta}$	pitch rate, radians/sec (fig. 1)
$\lambda_0$	nonrolling exponential damping constant, 1/sec
$\sigma$	radius of gyration, ft
$\dot{\phi}$	roll rate, radians/sec (fig. 1)
$\dot{\psi}$	yaw rate, radians/sec (fig. 1)
$\omega$	angular frequency of oscillation, radians/sec

DECLASSIFIED

CONFIDENTIAL

5

## VEHICLE DESCRIPTION

### Complete Configuration

A drawing of the Little Joe configuration is shown in figure 2 and a photograph of the vehicle ready for launching is presented as figure 3. The vehicle consisted of three major sections: The launch vehicle which housed the propulsion motors and the destruct system; the spacecraft, a full-scale model of the Mercury spacecraft; and an escape system consisting of a production escape rocket motor and supporting structure.


These three major sections were coupled by means of Marman clamps as shown in figure 2. These clamps, which were ring shaped, consisted of three segments of equal length held together with explosive bolts. An insulated fairing was bolted over each clamp to provide protection from aerodynamic forces and heating.

The weights of the various vehicle components are as follows:

Escape system (includes 236 pounds of ballast), lb . . . . .	1,015
Upper Marman clamp, lb . . . . .	18
Spacecraft, lb . . . . .	2,386
Lower Marman clamp, lb . . . . .	53
Launch vehicle, lb . . . . .	40,064
Total weight of vehicle at launch, lb . . . . .	43,536

### Launch Vehicle

The launch vehicle section consisted of a body section, a fin assembly, and an adapter section as shown in figure 2. The body section was constructed of 0.1-inch aluminum through the application of monocoque structural design and housed the cluster of eight solid-propellant rockets. The propulsion system for this test consisted of four XM-33E2 Castor rocket motors and four XM-19E1-C12 Recruit rocket motors. Pertinent characteristics of the motors are given in table I. The launch-vehicle shell was assembled on the launcher and the rocket motors installed as described in reference 2. The four Castor rocket motors and the four Recruit rocket motors were mounted in short tubes in the rear body structure. The Recruit motor nozzles were canted  $12^{\circ}$  and the Castor motor nozzles were canted  $11^{\circ}$  so that their thrust axes passed through a point approximately halfway between the centers of gravity for the loaded and burned out conditions. The fin assembly consisted of four wedge-shaped fins fabricated from aluminum alloy. The adapter section was fabricated from 3/16-inch aluminum and was riveted to the forward end of the body section.



CONFIDENTIAL

A more complete description of the Little Joe with pictures showing its assembly is presented in reference 2. The present launch vehicle was altered in some respects from the one described in this reference. For this test, portions of the skirt which extended rearward of the base were removed. The base of the launch vehicle, the inside of the skirts, the rocket nozzles, and the trailing edge of the fins were coated with approximately 1/8 inch of silicone rubber. Steel cover plates (1/8 inch thick) were bolted on the nozzle exits of the two second-stage Castor rockets. The purpose of the silicone rubber coating and the steel cover plates was to protect these portions of the launch vehicle from the heating produced by the rocket exhausts and thus to preclude structural failure or preignition of the grain in the second-stage motors. In a previous test of one of the Little Joe vehicles noncatastrophic pre-ignition of the two second-stage motors occurred. (See ref. 2.)

A pressure plate made of magnesium and having the same general shape as the spacecraft heat shield was bolted on the forward end of the adapter. This plate structurally stiffened the adapter and uniformly distributed the loads between the adapter, the Marman clamp, and the spacecraft. It was also intended to protect the spacecraft from the force of the destruct-system explosion in the event of destruct-system actuation.

### Spacecraft

The spacecraft used in this test was designed and constructed at the Langley Research Center. The geometric configuration of the spacecraft was essentially that of the Mercury spacecraft; however, the structural materials were different. A drawing of the spacecraft is presented in figure 4. The spacecraft consisted of four main sub-assemblies: the heat shield, the pressure compartment, the afterbody, and the antenna section.

The ablative heat shield was a fiber-glass spherical segment designed to sublime at 500° F. It varied in thickness from 1.06 inches at the center to 1.80 inches near the outer edge.

The pressure compartment was made of 0.2-inch-thick fiber glass. This portion of the spacecraft housed oscillograph recorders, telemeter components, a biological package, and the major portion of the instrumentation. Located on the external sides of the pressure compartment were two fiber-glass camera pods which protruded beyond the circumference of the heat shield. The external surface of this pressurized section and the camera pods were coated with 0.1 inch of a low-temperature ablative material made by Emerson Electric Manufacturing Company and designated as Thermo-lag. This material was sprayed on and cured in layers of about 0.01 inch until a thickness of 0.10 inch was

CONFIDENTIAL

CONFIDENTIAL

7


obtained. This material had previously been tested in the ethylene-heated high-temperature jet at NASA Wallops Station to determine its suitability for this application. It was an ablative material in which the resins sublimed when exposed to temperatures above 230° F and left a charred residue. For this flight the Thermo-lag was also covered with a sprayed-on plastic coating to prevent it from absorbing moisture prior to launch.

L  
1  
3  
5  
0  
The afterbody section was of single-wall construction and was corrugated as indicated in the sketch in the lower part of figure 4. These corrugations were intended to strengthen the outer skin and enable it to withstand the aerodynamic loads imposed during the flight. The cylindrical upper part was made of 1/32-inch-thick Inconel, and the sloping conical part was made of 0.05-inch-thick Inconel. For simplification, most of the structural members inside the spacecraft are not shown in the sectional side view of figure 4. Located in this conical portion of the afterbody was the flight-events sequence programmer.

The antenna-housing section, located above the afterbody section on top of the spacecraft, housed the drogue parachute and covered the antennas for the beacons used as part of the recovery aids. The construction of this section was similar to that of the afterbody section and was made of 1/32-inch-thick corrugated Inconel. The upper end of this section, which was protected with a blast shield during the first 69 seconds of the flight, was made of 1/4-inch fiber glass.

#### Escape System

A drawing of the escape system is presented in figure 5. This system was fitted to the spacecraft as shown in figure 2. The thrust axis of the escape rocket was misaligned about 1 inch to the side of the spacecraft—escape-system center of gravity to make certain that this part of the configuration would be pulled out of the flight path of the launch vehicle. The attitude sensor shown on the forward end of the escape rocket was arranged to measure pitch and yaw attitudes. The Grand Central Rocket Company escape rocket (1-KS-52000), which had a solid-propellant grain, was designed to produce a nominal thrust of 52,000 pounds for about 0.78 second. The Atlantic Research Corporation tower-jettison rocket (1.4-KS-785) mounted at the rear center of the Grand Central rocket was designed to produce a nominal thrust of 785 pounds for about 1.3 seconds. The pertinent characteristics of these motors are given in table I. The legs and braces of this structure were made of 2-inch- and 1-inch-diameter heavy-duty stainless-steel tubing, respectively. The entire escape-system assembly was composed of current production Mercury components.





CONFIDENTIAL

## Instrumentation


The Little Joe vehicle was extensively instrumented in order to determine its performance during the flight and to monitor expected flight events. A listing of the information obtained and the recording technique follows:

1. A recording oscillograph was used for primary spacecraft motion measurements

- (a) High-range accelerations (each axis)
- (b) Low-range accelerations (each axis)
- (c) Angular velocity (about each axis)
- (d) Angular attitude (each axis)

L  
1  
3  
5  
0

and for research data and monitored information

- (e) Drogue parachute deployment
  - (f) Seven spacecraft surface temperatures (thermocouples)
  - (g) Spacecraft air temperature
  - (h) Spacecraft internal wall temperature
  - (i) Spacecraft internal pressure
  - (j) Strain-gage supply voltage
  - (k) Three camera frame counters
  - (l) Time (onboard timer)
  - (m) Radiation (Geiger-Müller rate instrument)
  - (n) Control-system pressure
  - (o) Spacecraft Marman band release
  - (p) Spacecraft separation
  - (q) Tower Marman band release
- 

CONFIDENTIAL

9

(r) Drogue parachute cover separation

(s) Main parachute deployment

2. A mechanical-type pressure recorder for pressure survey measurements as obtained by 10 surface-located orifices was used.

3. An NASA eight-channel FM/AM telemeter was used to transmit the following information:

(a) Accelerations (each axis)

(b) Angle of attack (to spacecraft-tower separation)

(c) Angle of sideslip (to spacecraft-tower separation)

(d) Events (same as those listed as items 1(o) to 1(s))

(e) Time (onboard timer)

4. A two-channel tape recorder was used for noise measurements.

5. A Geiger-Müller rate-measuring instrument was used to measure the rate of radiation (item 1(m)). This system consisted of a transistorized circuit using an Anton 114 thin-wall counter tube in the Geiger-Müller instrument. In order to measure the total dosage of radiation, five film dosimeters with different filters and four self-reading capacitor dosimeters were used. The location of these radiation-measuring instruments is indicated in the section entitled "Results and Discussion."


6. Onboard cameras were located in two pods on the conical section of the spacecraft as follows:

(a) One upward-pointing camera

(b) One sideward-pointing camera

(c) Two downward-pointing cameras

Location of pressure orifices and thermocouples will be noted in a subsequent section where data from these sources are presented. Both oscillograph-recorded and telemetered accelerometers were mounted inside the pressurized section to measure normal, transverse, and longitudinal accelerations along the spacecraft axes. The attitude of the spacecraft in pitch, yaw, and roll was sensed by three attitude gyros. Pitch, yaw, and roll velocities were measured by rate gyros.



CONFIDENTIAL

## Biological Package

In addition to the NASA instrumentation onboard the spacecraft, the School of Aviation Medicine, USAF, provided a self-contained biological package (hereafter referred to as biopack), which contained a live rhesus monkey with several biological specimens such as insect eggs and larvae attached to the outside of the biopack. This container, which was of fiber-glass construction and cylindrical in shape, was 18 inches in diameter and 36 inches long. The biopack was sealed and had a life-sustaining atmosphere for the monkey of 56 hours.

The monkey was snugly laced in a form-fitting couch (see fig. 6), which left his arms free and afforded him limited head freedom. An 11-channel oscillograph recorder, located in the spacecraft external to the biopack, provided a permanent record of data pertaining to the physiological reactions of the monkey to the flight conditions and his reaction to a programed psychomotor test.

The 11 channels for the biopack were as follows:

Three electrocardiographs

Two nystagmus (one each for the horizontal and vertical eyeball motion)

One biopack internal air temperature

One air total pressure

One oxygen partial pressure

One relative humidity

One respiration rate

One psychomotor-test monitor

In addition, a motion-picture camera was mounted in the biopack to obtain a photographic record of the monkey's face.

A detailed description of the biopack system and the way in which its life-support features functioned is presented in reference 3. Post-flight inspection indicated that the biopack life-support system functioned quite well and that the rhesus monkey withstood the forces encountered during the flight with no apparent physical harm.

CONFIDENTIAL

CONFIDENTIAL

11

### Destruct System

L  
1  
3  
5  
0

Mounted on the head cap of each of the four Castor motors was a Beckman and Whitley destructor unit containing an annular-shaped charge. When these charges ignite, cores about 10 inches in diameter are cut from the head caps of the motors to allow the propellant exhaust gases to discharge through the forward end of the motors. The destruct system also included an FRW-2 ground command transmitter and two Avco Crosley Corporation receivers no. AD-183107 which were mounted in the adapter section.

### Control System

Automatic control of the spacecraft, which was initiated after escape-system jettisoning, was provided by a system consisting of reaction jet controls and a Minneapolis-Honeywell autopilot which provided the intelligence for the operation of the reaction jets. The autopilot had the capability of sensing and responding to angular attitudes as well as angular rates about the pitch, yaw, and roll axes. However, because of the sequence of separation events selected for this flight in keeping with the objectives thereof, the rate damping mode only was employed. Through the use of a "g" sensitive switch, operation of the control system was terminated at 0.05g deceleration during entry.

The autopilot was mounted on a bridge over the biopack in the pressurized section of the spacecraft. The control jets were located on the periphery of the pressurized compartment near the base of the spacecraft as shown in figure 4.

### LAUNCH FACILITIES

The Little Joe vehicle was launched from the NASA Wallops Station. Range clearance was obtained for an area bounded on the north by a line bearing 130° true from Wallops Island and on the south by a line bearing 155° true from the same location. Range limitation was 250 nautical miles from Wallops Island.

The Instrument Control Center building and launcher were situated close to the Atlantic Ocean side of the island. Located inside the aforementioned building was the equipment necessary to remotely control the launch, record telemetered data from the vehicle, and initiate destruct if the vehicle, during boost, veered too far off the intended trajectory. As a detection aid in the event that this situation occurred before acquisition by the space radars, a skyscreen was employed. This skyscreen, a gridded network through which the early portion of the

[REDACTED]

CONFIDENTIAL

flight could be visually monitored for variations in the vertical plane, was located about 1 mile south of the launcher.


The launcher served as an assembly fixture at the launch site and as a platform, remotely adjustable in elevation and azimuth, for the launching. (See fig. 3.) It was constructed of steel and was rugged enough to withstand the effects of operational use and inclement weather over an extended period of time. The launcher was designed for a movement in elevation from  $90^{\circ}$  vertical to  $70^{\circ}$  and provided for a range of travel in azimuth of  $90^{\circ}$ . A complete description of the launcher and its assembly is given in reference 4.

Radar tracking of this flight was provided by three space radars (SCR-584, AFMTC Mod II, and AN/FPS-16) and one velocity radar (CW Doppler velocimeter) on Wallops Island and a long-range radar at the M.I.T. Lincoln Laboratory located at Millstone Hill, Massachusetts.

Photographic coverage consisted of one fixed and three 16-millimeter tracking cameras and two 35-millimeter tracking cameras at several camera stations on Wallops Island along with a long-range 35-millimeter tracking camera at a camera station on the Eastern Shore of Virginia approximately 18 miles south of Wallops Island. Launch-vehicle take-off and spacecraft separation were filmed by cameras onboard three Air Force T-33 airplanes. In addition, the ships and airplanes of the recovery force were prepared to photograph the spacecraft during recovery.

#### TEST TECHNIQUE

A nominal no-wind trajectory for an elevation angle of  $82^{\circ}$  and an azimuth of  $140^{\circ}$  true was calculated for the Little Joe vehicle. Studies of the effects of wind on the vehicle were made in order to determine corrections necessary to cause the actual trajectory to coincide with the calculated trajectory. Trajectories were computed on an IBM 704 electronic data processing machine for these studies by a method which involved three-dimensional trajectory simulation (six degrees of freedom) with arbitrary winds. It was found that the wind effects on the vehicle were appreciable only for the first 10 seconds of flight. By using measured wind data obtained about 45 minutes prior to launch, it was determined that an elevation angle of  $78^{\circ}$  combined with an azimuth angle of  $157^{\circ}$  should give the same flight-path angle as the calculated no-wind trajectory at 10 seconds. The launcher was then set at these elevation and azimuth angles. About 15 minutes before launch, new wind data were obtained. It was found that the winds had changed sufficiently to dictate a new setting of the launcher. However, because of overriding operational considerations a decision was made to launch the vehicle without making these final adjustments to the launcher



CONFIDENTIAL

13

settings. Hence, the vehicle did not attain the expected altitude for a no-wind trajectory for a launch angle of  $82^{\circ}$  and the flight-path angle at 10 seconds was less than that estimated for the aforementioned conditions by approximately  $5^{\circ}$ . The method of correcting launcher azimuth and elevation angles for wind effects, which was used in this flight test, is presented in detail in reference 5.

L  
1  
3  
5  
0  
At launch, the four Recruit rocket motors and two of the Castor rocket motors ignited to give a thrust of about 260,000 pounds. The Recruits burned out after about 2 seconds and the two Castors burned out at about 30 seconds. The remaining two Castors ignited at 23 seconds giving an overlap of about 7 seconds for the two stages. These last two Castors then thrust until 58 seconds. At approximately 59 seconds, the escape motor ignited and pulled the spacecraft away from the launch vehicle. At about 69 seconds the escape-system rocket with its supporting tower was separated from the spacecraft by means of a jettison rocket. The spacecraft then continued along a ballistic path, achieving a maximum altitude of about 53 statute miles. At about 6 minutes and 13 seconds the drogue parachute deployed at an altitude of 20,200 feet. About 35 seconds later the main parachute deployed at an altitude of approximately 10,100 feet. The spacecraft impacted in the Atlantic Ocean 11 minutes 16 seconds after launch and at a range of 169 nautical miles from Wallops Island. Information relative to the recovery of the spacecraft is presented in the succeeding section.

As noted in the section entitled "Instrumentation," there was some duplication of instruments between the onboard oscillograph recorder system and the telemeter system to insure the availability of the more important data in case the spacecraft could not be recovered.

The three space radar units mentioned in the section entitled "Launch Facilities" were used to skin-track the vehicle to provide slant range, azimuth, and elevation angle. From these data, altitude, horizontal range, flight-path angle, and velocity were computed. A rawinsonde, released shortly after the flight, provided measurements of pressure and temperature up to 88,000 feet, which made it possible to determine air density. Above this altitude, the ICAO standard atmosphere (ref. 6) was assumed. Wind characteristics aloft, which were used in making wind corrections to the velocity data, were obtained through radar tracking of the rawinsonde.

The CW Doppler radar unit measured vehicle velocity from 3.4 seconds to 39.6 seconds after launch. Velocity data obtained from the Mod II and FPS-16 radars agreed closely with the Doppler data and were used in conjunction with information from the rawinsonde to obtain Mach number and dynamic pressure.

C [REDACTED]

CONFIDENTIAL

Space radar tracking did not yield usable information beyond 210 seconds of flight. Therefore, after this time recourse was made to a calculated trajectory for which the measured accelerations were considered.

The type of trajectory considered was that of a point mass. Since the objective of this program was simply to extend the trajectory of the spacecraft beyond 210 seconds, initial conditions for the start of the computer program were selected at apogee (170 seconds after launch) where the flight-path angle was zero. Time histories of the acceleration along the three spacecraft axes (axis system shown in fig. 1) as obtained by onboard instrumentation were used first to obtain an acceleration normal to the longitudinal axis of the spacecraft; this acceleration was the resultant of the normal and transverse accelerations. This resultant normal acceleration was then used in conjunction with the longitudinal acceleration to obtain an acceleration along the velocity vector. This acceleration  $a_D$  was computed by means of the expression

$$a_D = a_L \cos \eta + a_R \sin \eta$$

The angle  $\eta$  is the angle between the vectors for  $a_D$  and  $a_L$ , or the angle between the resultant relative wind and the longitudinal axis. Since plots of wind-tunnel data in the form of  $C_N$  as a function of  $\eta$  and  $C_A$  as a function of  $\eta$  were available, it was possible to obtain the variation of the ratio  $C_N/C_A$  with  $\eta$ . However, as it was necessary to determine  $\eta$  independent of the dynamic pressure since it was a desired instead of a known quantity, the ratio  $a_R/a_L$  had to be used rather than the ratio  $C_N/C_A$  in obtaining  $\eta$  values from the aforementioned wind-tunnel data. Brief time histories of  $a_D$ ,  $C_D$ , and  $\eta$ , consisting of about two cycles each, were plotted for the purpose of obtaining average values of these quantities over small time increments. The acceleration  $a_D$  and the drag coefficient were inputs to the digital trajectory simulation along with initial conditions at the apogee of the trajectory. Some of the outputs of the machine computation were the ratio of air density along this simulated trajectory to the density of air as obtained from the ARDC Model Atmosphere of 1959 (ref. 7), velocity, Mach number, dynamic pressure, flight-path angle, altitude, and range. The density ratio was then compared with a band of density ratio which had been established as defining what were considered reasonable limits on the variation of density. Several additional digital computer "runs" were made with slight refinements being made to the input data for each repeat run. The computed entry trajectory selected for this flight was considered a good representation of the actual trajectory. This is substantiated to a considerable degree by a comparison

CONFIDENTIAL

15

of the altitude at drogue parachute deployment as obtained from spacecraft instrumentation (20,200 feet) with the altitude at drogue parachute deployment yielded by the digital computer (21,000 feet).

## RECOVERY

Responsibility for spacecraft recovery was assigned to the Commander-in-Chief of the Atlantic Fleet of the U.S. Navy who, in turn, designated the Commander of Destroyer Flotilla Four as recovery operations commander. The air and surface support consisted of two P2V airplanes, four helicopters, two destroyers, one Landing Ship Dock (LSD), and a sea-going tug. Two of the helicopters were stationed at Wallops Island and the other two were aboard the LSD.

To assist in locating the spacecraft following impact in the Atlantic Ocean, several onboard recovery aids were employed. Two Sarah beacons, activated at main parachute deployment, were used to serve as homing transmitters by which the spacecraft could be located through the use of receivers onboard the P2V airplanes and the surface vessels. These beacons had an expected lifetime of 24 hours. The telemeter transmitter used during flight for data transmission was allowed to operate after impact as a backup for the Sarah equipment.

Two Sofar bombs were provided, one to be released at main parachute deployment with detonation to occur at a water depth of 2,800 feet and the other to remain onboard the spacecraft and set to detonate also at a depth of 2,800 feet if the spacecraft sank. This would provide an indication of such an occurrence to the listening devices which were monitoring these bombs.

Two bags of green fluorescein were located behind the spacecraft heat shield. Shortly after impact the contents of the bags became saturated with sea water and emanated green dye which discolored the water in the vicinity of the spacecraft. This dye, which had an expected lifetime of 15 hours, was an aid in establishing visual contact with the spacecraft from the air.

In addition to the aforementioned aids a flashing light, activated at main parachute deployment, was provided which had an operating lifetime of approximately 24 hours.

Location of the spacecraft was effected by one of the P2V airplanes which received a signal from the Sarah beacons at a distance of 94.5 nautical miles from the spacecraft and obtained a fix on its position. The airplane then radioed this position information to a destroyer which was dispatched to the designated position. After reaching the vicinity of

CONFIDENTIAL



CONFIDENTIAL

the spacecraft, ship's personnel saw the dye marker before sighting the spacecraft. The spacecraft was subsequently recovered and secured onboard the destroyer USS Borie in  $1\frac{3}{4}$  hours after launch.


## RESULTS AND DISCUSSION

### Trajectory

The trajectory as presented in figure 7 in the form of altitude plotted against time and in figure 8 as altitude plotted against horizontal range was obtained from space-radar tracking up to 210 seconds. Beyond this time, the trajectory shown as long dashes is that which was obtained from digital computation as indicated in the section entitled "Test Technique." With the exception of the first portion of flight up to approximately 60 seconds and the last portion after 280 seconds, the spacecraft traversed a ballistic flight path reaching apogee of 279,000 feet at 170 seconds. Weightlessness existed for approximately 2.5 minutes. As can be seen in figure 7 the agreement between the desired trajectory (nominal no-wind trajectory for a launch elevation angle of  $82^{\circ}$ ) and the actual trajectory is not close after 50 seconds. However, it should be remembered, as pointed out in the section entitled "Test Technique," that operating circumstances did not permit final corrections to the launcher which were dictated by changes in wind magnitude and direction prior to launch. Therefore, an evaluation of the method of correcting for wind effects based on results from this flight would not be justified here.

The occurrence of significant flight events is noted on figure 8. The sinking rate of the spacecraft following drogue parachute deployment varied from about 300 feet per second at an altitude of 20,200 feet to about 260 feet per second at an altitude of 10,100 feet. The sinking rate following main parachute deployment varied from about 41 feet per second at an altitude of 10,100 feet to about 35 feet per second at sea level. This rate at sea level was higher than the anticipated impact velocity of 30 feet per second.

The velocity time history is shown in figure 9. The maximum acceleration imparted to the spacecraft during boosted flight occurred at approximately 25 seconds, several seconds after second-stage ignition. However, the spacecraft experienced its maximum acceleration of  $14.9g$  during the firing of the escape-system rocket. The maximum velocity of 5,725 feet per second was attained by the spacecraft at the end of escape-rocket burning.



CONFIDENTIAL

17

Dynamic pressure variation with time is also presented in figure 9. The vehicle encountered maximum dynamic pressure of 2,980 pounds per square foot at 31 seconds followed by a rapid decline in pressure from this time to 59 seconds when the firing of the escape rocket added 100 pounds per square foot to the dynamic pressure. This slight increase was followed by a rapid decrease in dynamic pressure to essentially zero as the spacecraft approached the apogee of its trajectory. During entry, dynamic pressure increased to a peak value of 240 pounds per square foot followed by a decline to a level of approximately 120 pounds per square foot for about 50 seconds prior to drogue parachute deployment.


Figure 10 presents the variation of flight Mach number with time. The maximum Mach number achieved by the complete configuration was 5.25 whereas the peak Mach number experienced by the spacecraft was 5.70, the increase being imparted by the escape rocket. Entry Mach number was approximately 4.25 based on the time at which the dynamic pressure began to increase discernibly. The scale of the flight test in the form of Reynolds number per foot is also shown in figure 10 along with Mach number.

#### Operation of Escape System

As indicated in the introduction, qualification of the escape system was one of the primary considerations of this flight test. Since the trajectory conditions of low dynamic pressure and peak Mach number were the governing parameters for the initiation of escape-system operation, prefiring trajectory studies were made to determine when these criteria were likely to occur. Prior to launching the vehicle, this time was programed into a timer onboard the capsule. The time selected for release of the main Marman band and ignition of the escape rocket was 59 seconds from the time of launch. An inspection of the flight record indicated that these two events occurred just 0.02 second prior to the anticipated time. During burning of the escape rocket a longitudinal acceleration increment of 14g was imparted to the spacecraft.

Static stability of the escape configuration during burning of the rocket motor was determined from the period of the motion. The motion was stable with the derivative  $C_{m\alpha}$  being approximately -0.0057 at a Mach number of 5.5. This value indicates a reduction in static stability, when compared with power-off wind-tunnel results reported in reference 8, of about 45 percent during the burning of the escape rocket motor.

After burnout of the escape rocket, the spacecraft, tower, and spent rocket-motor combination coasted until 69.4 seconds from launch. At this time the Marman band, which coupled the spacecraft and the tower-rocket-motor combination, was released and the jettison rocket mounted at the



CONFIDENTIAL

base of the escape rocket between the three nozzles was fired, thereby separating the tower and rocket-motor case from the spacecraft. As can be seen in figure 8, the spacecraft then coasted to an altitude of 279,000 feet.

It was planned that a pressure-sensitive switch, which was used in conjunction with a manifolded ring of six evenly spaced orifices near the middle of the cylindrical section, would initiate drogue parachute deployment at 20,000 feet. The pressure-sensitive switch was to close a circuit which would cause release of the mechanical attachment that retained the drogue parachute cover and would fire a mortar to push the parachute out of its canister. An examination of the flight record indicates that drogue cover release occurred at 372.5 seconds (from launch) followed by mortar firing 0.8 second later. This corresponded to an altitude of 20,200 feet.

Main parachute deployment, which was planned for 10,000 feet, was also initiated by a switch set to be sensitive to the static pressure expected at that altitude. Deployment took place at 408.2 seconds (from launch) which, according to the pressure records, corresponded to an altitude of approximately 10,100 feet. The main parachute provided a descent rate sufficiently low (approximately 35 feet per second at sea level) for the spacecraft to make a nondestructive ocean impact.

Thus, the results relative to the escape system obtained from the flight test demonstrate the soundness of the system concept at the trajectory condition of low dynamic pressure (and high altitude) since the acceleration during escape-rocket burning was within the limits of human tolerance for the supine position as cited in references 9 and 10, that the escape configuration remained stable although experiencing a reduction in static stability during rocket burning, and that the sensing and actuating devices of the system functioned at the desired times or altitudes.

#### Entry Motion

As indicated in the section entitled "Instrumentation," the spacecraft was equipped with, among other items, three angular rate gyros and three linear accelerometers. Data from these sources were employed in an analysis of spacecraft motions during entry. Presented in figure 11 are typical time histories of the spacecraft entry motion data for a supersonic and subsonic Mach number. Flight measurements shown are transverse, normal, and longitudinal accelerations and pitch, yaw, and roll rates. Since the spacecraft was rolling, although at a relatively low rate, the approach to analysis of the spacecraft motions was made through cross plots of pitch rate and yaw rate. This cross plotting was done over a time range sufficiently large to obtain three to four

CONFIDENTIAL

cycles in each time increment considered. From these plots vector distances of the various points as measured from the trim center were determined which represented the resultant oscillatory angular rate of the spacecraft. These graphically determined values were then plotted against time to obtain a time history of the resultant angular rate. The maximum amplitude of this angular rate measured from the middle of the envelope of the oscillations was then used in the following expression for the maximum resultant angle of attack  $\alpha_{R,max}$ :

$$\alpha_{R,max} = 57.3 \frac{\dot{\alpha}_{R,max} P}{2\pi}$$

The times at which  $\dot{\alpha}_{R,max}$  occurred agreed quite well with the occurrence of zero values of normal and transverse acceleration, an indication that at these times the spacecraft was passing through zero angle of attack. Therefore, this was the proper reference point from which to establish the time of maximum resultant angle of attack as being a quarter of a period later than  $\dot{\alpha}_{R,max}$  since the angle is  $90^\circ$  out of phase with the angular rate. The maximum resultant angle of attack obtained in the aforementioned manner is presented in figure 12 plotted against altitude during entry. For the purpose of orientation it should be noted that these values represent the maximum angular deviation of the spacecraft axis from the flight path when descending heat shield forward. The maximum angle of attack of approximately  $100^\circ$  occurred at an altitude of 40,000 feet. It can be seen that although the spacecraft oscillated through extremely large angles it did not tumble during entry. The trend of the variation of the maximum resultant angle of attack with altitude shown in this figure is quite similar to that of the theoretical nondimensional angle of attack presented in figure 1 of reference 11 for a positive value of the "dynamic-stability" parameter denoted therein as  $k_1$ . The value of  $k_1$  for the spacecraft was found through the use of experimental values of the dynamic stability factor

$$C_D - C_{L\alpha} + (C_{mq} + C_{m\ddot{\alpha}}) \left( \frac{l}{\sigma} \right)^2$$

from reference 12, to be positive also and of the same order of magnitude.

### Spacecraft Stability

From the oscillatory time histories of the resultant angular rate, which were obtained in conjunction with the analysis described in the previous section, it was possible to determine the period of the oscillatory motion. This period is presented in figure 13 as a function of Mach

CONFIDENTIAL

CONFIDENTIAL

number. It can be seen that the frequency of oscillation did not exceed 1.0 cycle per second. The frequency, although varying from approximately 0.8 cycle per second to 0.3 cycle per second, remained close to the level of frequency (below 100,000 feet) shown in figure 10 of reference 13 as obtained in a theoretical study of the motion of a ballistic-entry body whose shape was similar to that of the spacecraft of this test. The pitch moments of inertia of the two bodies, although not identical, were of the same order of magnitude. The period of oscillation is proportional to the square root of the moment of inertia and, since the square root of the ratio of the inertia of the test spacecraft to that of the model of the theoretical study is close to unity, the comparison of test-frequency results with those from reference 13 for substantiation is valid.

Shown for comparison is the oscillatory period obtained through a digital computer analysis at several Mach numbers for which wind-tunnel measurements of aerodynamic coefficients were available as a function of angle of attack. Tunnel data from references 14 and 15 were employed in conjunction with trajectory information from this flight, at the appropriate Mach number, in the computer program. During the several seconds of problem time for each Mach number, the output of this program yielded, among other quantities, a transient response in angle of attack. The period of oscillation was measured from the time history of this transient response.

Since the static stability derivative  $C_{m\alpha}$  could not be obtained from the flight measurements by the slope method, the frequency of the oscillatory motion as obtained from figure 13 was employed in the computation of this derivative by use of the expression

$$C_{m\alpha} = - \frac{I_Y}{57.3qAd} (\omega^2 + \lambda_o^2)$$


In view of the fact that the exponential damping constant is quite small, as will be seen in a subsequent figure, it was omitted in this calculation. The results are presented in figure 14 where comparison is shown with data from reference 14 and reference 15. The flight results indicate that the spacecraft was statically stable in the entry attitude over the Mach number range of this test. In the subsonic and transonic region reasonably good agreement exists between the static stability obtained from the flight test and that obtained from the wind tunnel as reported in reference 14. For Mach numbers from 1.60 to approximately 3.00 there is a large discrepancy between the results of this test and those of the wind tunnel of reference 15. This difference could possibly be attributed to several reasons. First, it should be remembered that the values of  $C_{m\alpha}$  obtained from the flight test were computed from the average period of the resultant oscillatory motion and are therefore



representative of the average static stability of the spacecraft over a large range of angle of attack  $\alpha$  whereas the data of reference 15 were determined as the slope of the pitching-moment coefficient plotted against  $\alpha$  in the region of  $\alpha = 0^\circ$ . Also, it should be pointed out that the pitching moment of the spacecraft is nonlinear with angle of attack as shown in reference 15.

In an endeavor to substantiate flight-test stability results in the region of discrepancy with reference 15, the digital computer study mentioned in the discussion of the period of motion was undertaken. In view of the nonlinearity of the aerodynamic data and the very limited angle-of-attack range over which the slope was measured in references 14 and 15, it was considered possible that such a machine study would yield an oscillatory motion the period of which would be more representative of entry stability than that shown in reference 15 when the spacecraft is oscillating through large values of  $\alpha$ . It can be seen in figure 13 that good agreement exists between the period determined from flight data and that obtained from the computer study in which wind-tunnel measurements of aerodynamic characteristics and flight trajectory conditions are considered for the spacecraft in the entry attitude. Due to this favorable comparison of periods of oscillation, the flight-test results presented in figure 14 are considered to be a reasonable representation of the static stability of the spacecraft when it is oscillating through large angles of attack during entry. Reference 16 presents supersonic static stability of a spacecraft model as obtained from wind-tunnel tests employing a single-degree-of-freedom free-oscillation technique. It should be noted that the static-stability results presented in this paper as obtained from flight measurements were also determined from the characteristics of free oscillations. It can be seen in figure 14 that the flight results compare quite favorably with those from reference 16.

For the purpose of obtaining the dynamic stability characteristics of the spacecraft during entry, time histories of the resultant-force coefficient  $C_R$  obtained from cross plots of the normal-force coefficient  $C_N$  and the side-force coefficient  $C_y$  were analyzed. The approach to analyzing the time histories for  $C_R$  was through the logarithmic decrement technique by which values of the exponential damping constant were determined. The several values of the damping constant which it was possible to obtain by this technique are presented in figure 15. The exponential damping constant, which was quite small in magnitude, was negative over most of the entry Mach number range with the transition to positive values occurring at a Mach number of approximately 0.7. Thus, the spacecraft exhibited dynamic instability, although only to a very slight degree, throughout the greater portion of the entry trajectory. A further indication of this instability can be seen in figure 12, which has been discussed previously.



CONFIDENTIAL

### Drag


The drag coefficient of the spacecraft at zero lift during entry was determined by examining values of the normal and transverse accelerations to determine times at which these values were essentially zero. The coefficient was then computed by the use of the decelerations measured by the longitudinal accelerometer. The results are presented in figure 16 along with axial-force-coefficient results at  $\alpha = 0^\circ$  for subsonic and transonic speeds from reference 14 and at supersonic speeds from reference 15. It can be seen that agreement in the subsonic and transonic region between the flight results and those obtained from reference 14 is fair, with the greatest deviation being about 12 percent. It should be noted, as pointed out in reference 14, that the axial-force results presented therein have not been adjusted for base pressure and consequently are shown as gross values. At Mach numbers of 1.3 and 1.5 good agreement exists between data of this test and that from reference 17. With the exception of an inexplicable high flight-test value at  $M = 3.78$  and an abnormally low wind-tunnel value at  $M = 1.60$  from reference 15, which could not be explained therein, it can be seen that agreement of data from these two sources is good. Although the axial-force-coefficient data from reference 15 are uncorrected for base pressure, the chamber axial-force coefficients presented therein are quite small. The drag coefficient was essentially invariant with Mach number in the supersonic and hypersonic range at an average value of 1.55.

### Aerodynamic Heating

Temperature effects.- Temperatures were measured at seven locations on the inside wall of the spacecraft model. Time histories of the temperatures at these stations are given in figure 17. In comparing these time histories, it should be borne in mind that the materials and wall thickness were not the same for all parts of the model. A sketch of the model showing these materials and thicknesses is shown at the top of figure 17.

The temperature time history for the thermocouple at station 105.1 was low in comparison with that for some of the other stations because of the greater heat capacity of the material at this location, and also because this small end of the spacecraft was protected from the free stream and the escape-rocket blast by a blast shield. The blast shield (figs. 2 and 5) was in place up to the time that the escape system was jettisoned.

At station 80.2, the thermocouple was welded to the inside surface of a structural ring. Here again the temperature was low since this



CONFIDENTIAL

23

thermocouple was effectively mounted on an internal structural member as shown in view F-F of figure 17.


The thermocouples at stations 76.9, 62.0, 59.0, and 39.9 were welded to the inside peak of one of the corrugations as shown in figure 17. As shown in the figure, the Inconel skin thickness for the cylindrical section was 0.031 inch and for the conical section was 0.050 inch. The temperature on these ridge peaks was much higher than for any other location on the spacecraft.

At station 13.0, the thermocouple was cemented to the inside surface of a 0.2-inch fiber-glass wall which had a 0.1-inch ablative coating on the exterior surface as described in the section entitled "Vehicle Description." The temperature for station 13.0 did not exceed 110° F at any time as compared with a maximum of about 690° F for the other two stations (39.9 and 59.0) on the conical portion of the spacecraft. This large difference in maximum temperature can be attributed both to the increased heat capacity of this wall due to greater thickness at station 13 and to the heat protection provided by the ablative coating.

Postflight resistance measurements made on the ablative coating of the conical sidewalls indicated a char depth of 0.01 to 0.02 inch. Visual inspection after the flight showed that not only this surface but almost the entire surface of the spacecraft had the appearance of having been scorched.

No thermocouples were installed on the camera pods because of the limited number of telemeter channels available for instrumentation and also because the pods were constructed of thick fiber glass. It was anticipated that the camera pods would get very hot if unprotected from the free stream. Hence, they were also coated with 0.1 inch of the sprayed-on ablative material. The coating ablated all the way through to the fiber glass at several places on the pods and left a layer of carburized residue about the thickness of the original coating. At spots where the coating ablated all the way through, the charred residue blistered very severely and pulled away from the fiber glass. Probably sufficient heat passed through the residue at these spots to cause gases to escape from the fiber glass which in turn caused the covering residue to blister.

After the flight the heat shield appeared to be charred black over its entire exposed surface. This char was very thin (on the order of 0.01 inch) and could be easily removed. The heat shield was facing forward during most of the entry portion of the flight and hence took the major portion of the heat load. The effect of entry on the temperatures of other portions of the spacecraft can be seen in figure 17.





CONFIDENTIAL


The thermocouples on the cylindrical portion of the spacecraft indicated increased temperatures during entry whereas the ones on the conical portion did not show an increase. Unpublished data obtained during the free-flight entry testing of a Mercury spacecraft shape at Mach numbers up to 10 showed the heating on the cylindrical section and the parachute-canister section to be consistently greater than on the conical section. Apparently, when the heat-shield end was forward the flow was separated over the conical portion and then reattached on the cylindrical portion.

As indicated on figure 9, the escape-system rocket fired at 59 seconds. The motion pictures showed that the exhaust of this rocket impinged on the spacecraft to some extent. These jet impingements did not cause a temperature rise large enough to be noted on the temperature records even though one of the jets was aligned so that it would be almost directly upstream of the line of thermocouples on the spacecraft.

Comparison with theory.- Figure 18 presents a comparison of theoretical and measured temperatures for four stations on the spacecraft during the first 60 seconds of flight. During this time the spacecraft was essentially at  $0^\circ$  angle of attack with the small end forward. The Van Driest turbulent theory for a flat plate was used to calculate the theoretical temperatures. All lengths used in calculating the Reynolds numbers were measured from the corner of the small end of the spacecraft. The local flow conditions were calculated by using the surface pressures as measured during the flight and assuming the local total pressure to be equal to the stagnation pressure back of a normal shock. The free-stream static temperature was obtained from rawinsonde data.

Measured and theoretical temperatures for all the stations decreased slightly during the first few seconds after launch. The vehicle had been exposed to the sun for several hours before launch and had become hotter than the surrounding air.

During flight the measured temperatures did not rise as rapidly as the theory predicted. At 60 seconds after launch the measured temperatures on the cylindrical section were about one-half of those predicted by theory, and the measured temperatures on the conical section were about three-fourths of those predicted by theory. It should be noted that the spacecraft was not as aerodynamically clean as the sketch in figure 17 shows. The air through which the spacecraft was moving during these first 60 seconds had been greatly disturbed by the escape system mounted on the small end of the spacecraft. This escape system may have caused the boundary layer over the spacecraft to be thicker than theory would predict for an aerodynamically clean spacecraft or may have resulted in the spacecraft being completely or partially in separated flow which would have given rise to lower temperature and heat-transfer values than those predicted by theory. Regardless of the cause of the measured temperatures being less than the theoretical, a spacecraft




would be conservatively designed if it were constructed to withstand the theoretical temperatures.

### Pressure Measurements

Figure 19 presents the variation of local surface pressure with free-stream static pressure for nine stations on the spacecraft. The pressures are plotted in this manner to provide a visual comparison between the measured surface pressure and the free-stream pressure. The line on each plot is the line on which all the data points would have been if the surface and free-stream pressures had been equal throughout the flight. At launch, these pressures were all in good agreement within instrumentation accuracy as shown by the open symbols in the upper right-hand corner of each plot. During ascending flight, the surface pressures on the spacecraft sidewalls were generally greater than free-stream pressure. The pressure at station 71.2 was in agreement with this trend for the first three data points which were obtained during subsonic flight, but disagreed with this trend for the remaining portion of the ascending flight, which was supersonic. The pressure measurement at station 71.2 was obtained in a different fashion than those at other stations in that it was obtained from manifolding six orifices equally spaced around the spacecraft at this station. It should be noted that during the time these pressures were measured the spacecraft was not as aerodynamically clean as that shown by the sketch at the top of figure 19. During boost, an escape system was mounted on the small end with a bulging clamp just upstream of station 80.4. Also, during this time, the launch-vehicle adapter was fastened to the spacecraft at station 0 with a bulging clamp. During ascending flight the surface pressure on the base of the spacecraft was less than free-stream pressure for the first three data points, which were obtained during subsonic flight. After that, these pressures became greater than free-stream pressure due to the formation of shock waves in the supersonic flow ahead of the bulging clamp.

At 59 seconds, the escape rocket fired and the exhausting gases from this rocket impinged on the spacecraft and caused a small increase in some of the sidewall pressures. The maximum magnitude (0.5 pound per square inch absolute) and the duration (1.4 seconds) of this disturbance were small and hence are not shown on figure 19.

During the descending portion of the flight the spacecraft looked essentially like the sketch in figure 19 with the heat shield (large end) forward. The data for this entry period up to drogue parachute deployment are shown by solid symbols. The spacecraft was oscillating during entry with varying frequency and amplitude. The pressure traces on a recorder in the spacecraft indicated the same frequency of model oscillations as did accelerometer data. Since the heat shield was



CONFIDENTIAL

forward, the model oscillations caused the pressures on it to vary from free-stream to total-head values, and the agreement between the local and free-stream pressures for stations -3.0 and -9.2 in figure 19 was, in general, poor. However, since the sidewalls were in the wake of the heat shield, the model oscillations caused these pressures to vary only a maximum of about 0.75 pound per square inch absolute, and the agreement between the local and free-stream pressures was, in general, good.

In order for the parachutes in the spacecraft to deploy at the predetermined altitudes, a baroswitch was used to sense altitude and to be the signaling device for parachute deployment. It was desirable for the baroswitch to be able to sense a pressure on the spacecraft that would be a function of altitude regardless of the attitude of the spacecraft. Wind-tunnel testing had shown that a manifolded ring of pressure orifices near the middle of the cylindrical section would be suitable. Figure 19 shows that the manifolded pressures at station 71.2 were satisfactory since during entry the local surface pressure was in good agreement with the free-stream pressure and this agreement was constant regardless of the attitude of the oscillating spacecraft. As pointed out in the section entitled "Operation of Escape System" the drogue parachute deployed at an altitude of 20,200 feet as compared with a planned altitude of 20,000 feet. Also, the main parachute deployed at an altitude of 10,100 feet as compared with a planned altitude of 10,000 feet.


L  
1  
3  
5  
0

### Radiation Measurements

As was mentioned in the section entitled "Vehicle Description," cosmic-radiation-measuring instruments were a part of the spacecraft instrumentation. These were mounted inside the pressurized section as shown in figure 20. The dosimeters were mounted near the center of the spacecraft close to the biopack. The Geiger-Müller rate-measuring instrument was mounted near the outer wall of the spacecraft. This wall, as previously described, consisted of 0.2-inch fiber glass coated with 0.1 inch of Thermo-lag (a sprayed-on ablation material) on the outer surface. This instrument was mounted so that its radiation sensor was exposed to the radiation penetrating the spacecraft wall.

The dosimeters were of the type to measure total dosage of radiation. The total dosage during this test was so small relative to the film or capacitor sensitivities of the measuring instruments that it did not register on any of the dosimeters.

The radiation measured by the Geiger-Müller instrument is shown in figure 20. The altitude history is also shown in this figure to indicate the trends of radiation rate with altitude during this flight. The maximum rate of radiation of 0.4 milliroentgen per hour occurred



CONFIDENTIAL

27

at peak altitude. This rate is small in comparison with the allowable rate for personnel. The radiation measured by this instrument was essentially background cosmic radiation (primarily gamma type). This is the usual type of radiation encountered at the altitudes of this test. Beta particles, which usually exist at much higher altitude, would not have penetrated the spacecraft wall even had they been encountered.

### Noise Measurements

As was indicated in the section entitled "Instrumentation," noise measurements were made through the use of a two-channel tape recorder.

An example of the type of data obtained is the overall sound pressure level as a function of time shown in figure 21. Such events as lift-off, second-stage ignition, initiation of escape-system operation, and tower separation are identified. As a matter of interest, the maximum sound pressure level of 142 decibels occurs at approximately the time when the dynamic pressure is a maximum and is believed to be associated with the aerodynamic boundary layer on the outside surfaces of the vehicle. For the unprotected ear, studies of human tolerance to noise have shown the threshold of pain to be at 140 decibels. This should not be a cause for alarm with regard to the Mercury spacecraft since noise attenuation material has been incorporated into its design and fabrication and the astronaut's head gear will also afford some noise protection. Therefore, the aforementioned magnitude and noise tolerance level are cited merely as an indication of the noise environment against which protection must be provided.

For a more detailed description of the noise-acquisition equipment and analysis of the data therefrom the interested reader should consult reference 18.

### CONCLUSIONS

The third flight test in the Little Joe program, in which a rhesus monkey was successfully recovered, had as its primary objectives the qualification of the escape system at low dynamic pressure and high Mach number, the determination of aerodynamic characteristics of the spacecraft, and a study of spacecraft entry motions. From the results of this flight the following conclusions are made:

1. This test demonstrated the soundness of the escape-system concept at low dynamic pressure in that: maximum acceleration imparted to the spacecraft during escape-rocket burning was within the limits of

[REDACTED]

CONFIDENTIAL

human tolerance; the spacecraft-tower combination remained statically stable during rocket burning although a reduction in stability margin occurred; and the several sensing and actuating devices employed therein functioned as planned at the desired times or altitudes.

2. Although the spacecraft did not exhibit tumbling during entry, it oscillated through large angles which reached a maximum of approximately  $100^{\circ}$  at an altitude of 40,000 feet.

3. Analysis of spacecraft motions indicated that the spacecraft was statically stable although it exhibited a small degree of dynamic instability over the greater portion of the Mach number range of this test.

4. The drag coefficient of the spacecraft, large end forward, during entry was essentially invariant with the Mach number at supersonic and hypersonic speeds and was approximately equal to 1.55.


5. The fiber-glass sidewalls coated with a low-temperature ablative material experienced a maximum temperature of  $110^{\circ}$  F, whereas the Inconel sidewalls attained a maximum temperature of about  $700^{\circ}$  F.

6. The performance of the recovery aids was satisfactory, with location and recovery of the spacecraft being completed in  $1\frac{3}{4}$  hours from the time of launch.

7. The maximum rate of radiation (primarily gamma type) was 0.4 milliroentgen per hour and occurred at maximum altitude.

8. The maximum noise level was 142 decibels and occurred at approximately the time of maximum dynamic pressure.


Langley Research Center,  
National Aeronautics and Space Administration,  
Langley Air Force Base, Va., December 28, 1961.




CONFIDENTIAL

29

#### REFERENCES

1. Blanchard, Willard S., Jr., and Raper, James L.: Full-Scale Flight Test From Sea Level of an Abort-Escape System for a Project Mercury Capsule. NASA TM X-422, 1960.
  2. Royall, John F., and English, Roland D.: Investigation of Flight Performance of Little Joe Booster for Project Mercury. NASA TM X-298, 1960.
  3. Anon.: Escape Studies From Ballistic Space Vehicles. 61-29, School of Aviation Medicine, USAF Aerospace Medical Center (Brooks AFB, Texas), Apr. 1961.
  4. Anon.: Assembly and Maintenance Manual for Little Joe Project. MD 59-56, North American Aviation, Inc., May 15, 1959.
  5. Rose, James T., and Rose, Rodney G.: A Rapid Method of Estimating Launcher Setting to Correct for the Effects of Wind on the Trajectory of an Unguided Fin-Stabilized Rocket Vehicle. NASA TM X-492, 1961.
  6. Minzner, R. A., Ripley, W. S., and Condrion, T. P.: U.S. Extension to the ICAO Standard Atmosphere - Tables and Data to 300 Standard Geopotential Kilometers. Geophys. Res. Dir. and U.S. Weather Bureau, 1958.
  7. Minzner, R. A., Champion, K. S. W., and Pond, H. L.: The ARDC Model Atmosphere, 1959. Air Force Surveys in Geophysics No. 115 (AFCRC-TR-59-267), Air Force Cambridge Res. Center, Aug. 1959.
  8. Smith, Robert P., and Moseley, William C., Jr.: Static Longitudinal Stability Characteristics of Various Mercury Escape Configurations and of a Proposed Alternate Escape Configuration for Mach Numbers of 0.05 to 9.60. NASA TM X-494, 1961.
  9. White, Clayton S.: Biological Tolerance to Accelerative Forces. Convair Aeromedical Consultant's Rep., Lovelace Foundation for Medical Education and Res. (Albuquerque, N. Mex.), June 10, 1954. (Available from ASTIA as AD 158982.)
  10. Clarke, Neville P., Hyde, Alvin S., Cherniack, Neil S., and Lindberg, Evan F.: A Preliminary Report of Human Response to Rearward-Facing Re-Entry Accelerations. WADC Tech. Note 59-109, U.S. Air Force, July 1959.
- 

CONFIDENTIAL

11. Allen, H. Julian: Motion of a Ballistic Missile Angularly Misaligned With the Flight Path Upon Entering the Atmosphere and Its Effect Upon Aerodynamic Heating, Aerodynamic Loads, and Miss Distance. NACA TN 4048, 1957.
  12. Sommer, Simon C., Short, Barbara J., and Compton, Dale L.: Free-Flight Measurements of Static and Dynamic Stability of Models of the Project Mercury Re-entry Capsule at Mach Numbers 3 and 9.5. NASA TM X-373, 1960.
  13. Bird, John D., and Reese, David E., Jr.: Stability of Ballistic Reentry Bodies. NACA RM L58E02a, 1958.
  14. Pearson, Albin O.: Wind-Tunnel Investigation at Mach Numbers From 0.50 to 1.14 of the Static Aerodynamic Characteristics of a Model of a Project Mercury Capsule. NASA TM X-292, 1960.
  15. Shaw, David S., and Turner, Kenneth L.: Wind-Tunnel Investigation of Static Aerodynamic Characteristics of a 1/9-Scale Model of a Project Mercury Capsule at Mach Numbers From 1.60 to 4.65. NASA TM X-291, 1960.
  16. Fletcher, Herman S., and Wolhart, Walter D.: Damping in Pitch and Static Stability of Supersonic Impact Nose Cones, Short Blunt Subsonic Impact Nose Cones, and Manned Reentry Capsules at Mach Numbers From 1.93 to 3.05. NASA TM X-347, 1960.
  17. Rittenhouse, Lewis E., and Kaupp, Harry, Jr.: Experimentally Determined Static Stability and Drag Characteristics for NASA's Project Mercury Manned Orbital Capsule at Transonic Speeds. AEDC-TN-59-130, (Contract No. AF 40(600)-800), Arnold Eng. Dev. Center, Oct. 1959.
  18. Mayes, William H., Hilton, David A., and Hardesty, Charles B.: In-Flight Noise Measurements for Three Project Mercury Vehicles. NASA TN D-997, 1962.
- 

CONFIDENTIAL

TABLE I.- MOTOR CHARACTERISTICS FOR SEA-LEVEL CONDITIONS

Motor	Loaded motor weight, lb	Propellant weight, lb	Average thrust, lb	Web burning time, sec	Total burning time, sec	Impulse for web burning, lb-sec	Total impulse, lb-sec
Castor XM-33E2	8,777	7,300	53,340	27.00	40.00	1,437,000	1,607,000
Recruit XM-19E1-C12	354	268	36,300	1.52	2.50	55,295	60,990
Grand Central I-KS-52000	646	285	52,000	.78	1.39	40,500	56,500
Tower jettison I.4-KS-785	19.5	5.46	785	1.30	1.47	1,019	1,122





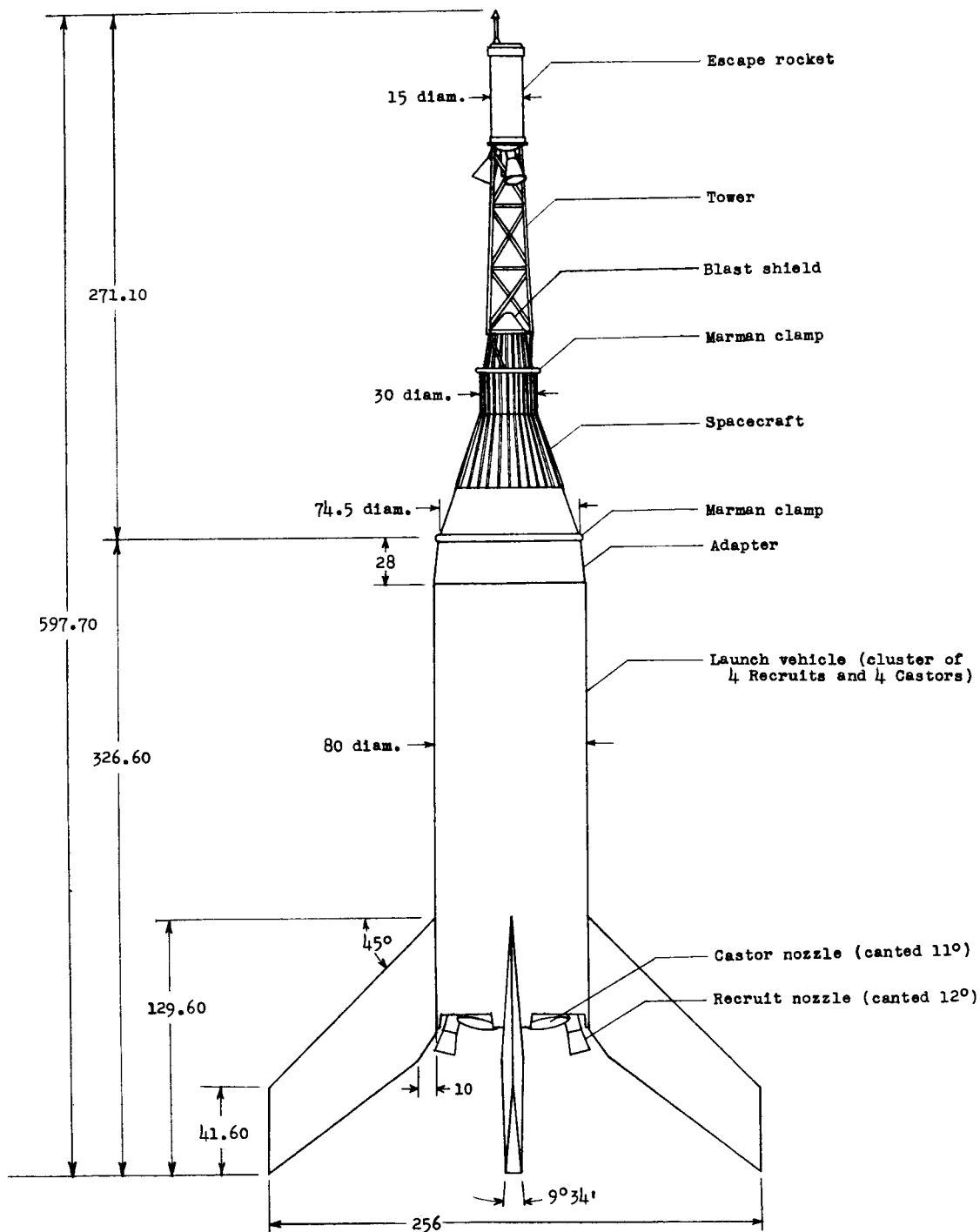
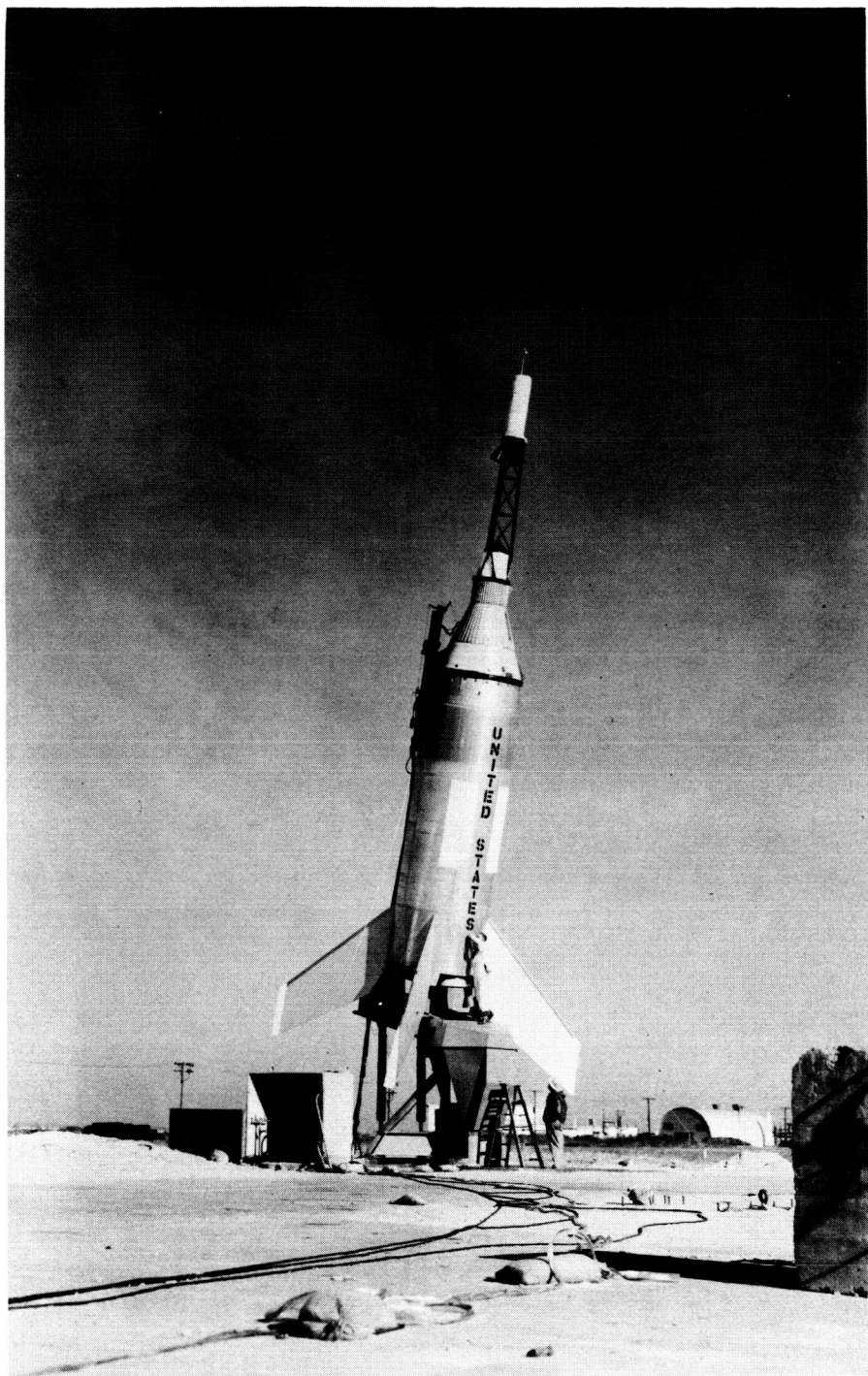


Figure 2.- Complete configuration of the Little Joe vehicle.  
All dimensions are in inches.

CONFIDENTIAL



L-59-8430

Figure 3.- The Little Joe vehicle ready for launching.

L-1350

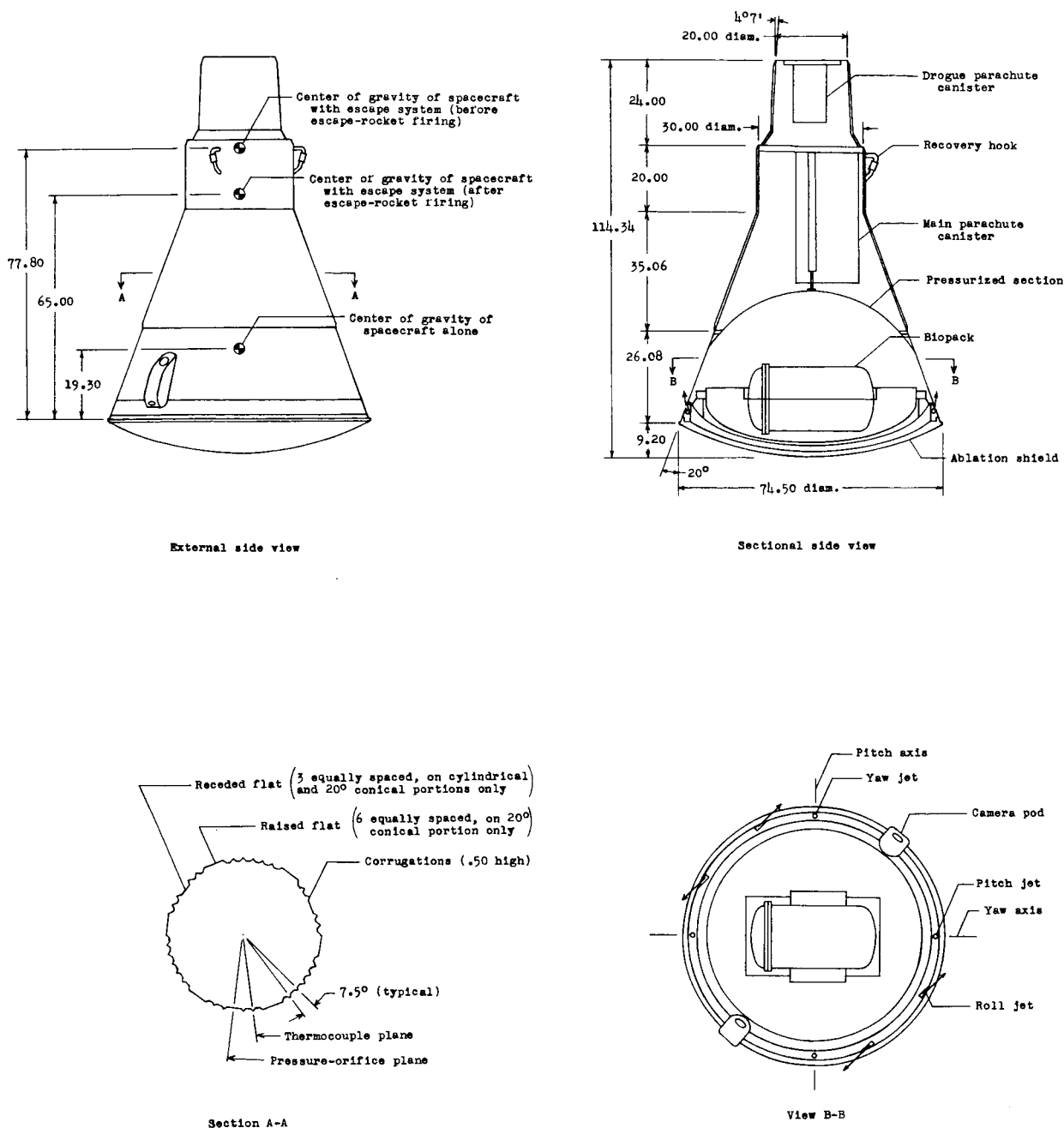


Figure 4.- Spacecraft details. All dimensions are in inches.

CONFIDENTIAL

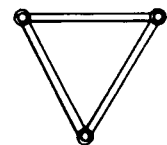
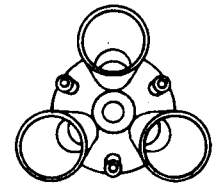
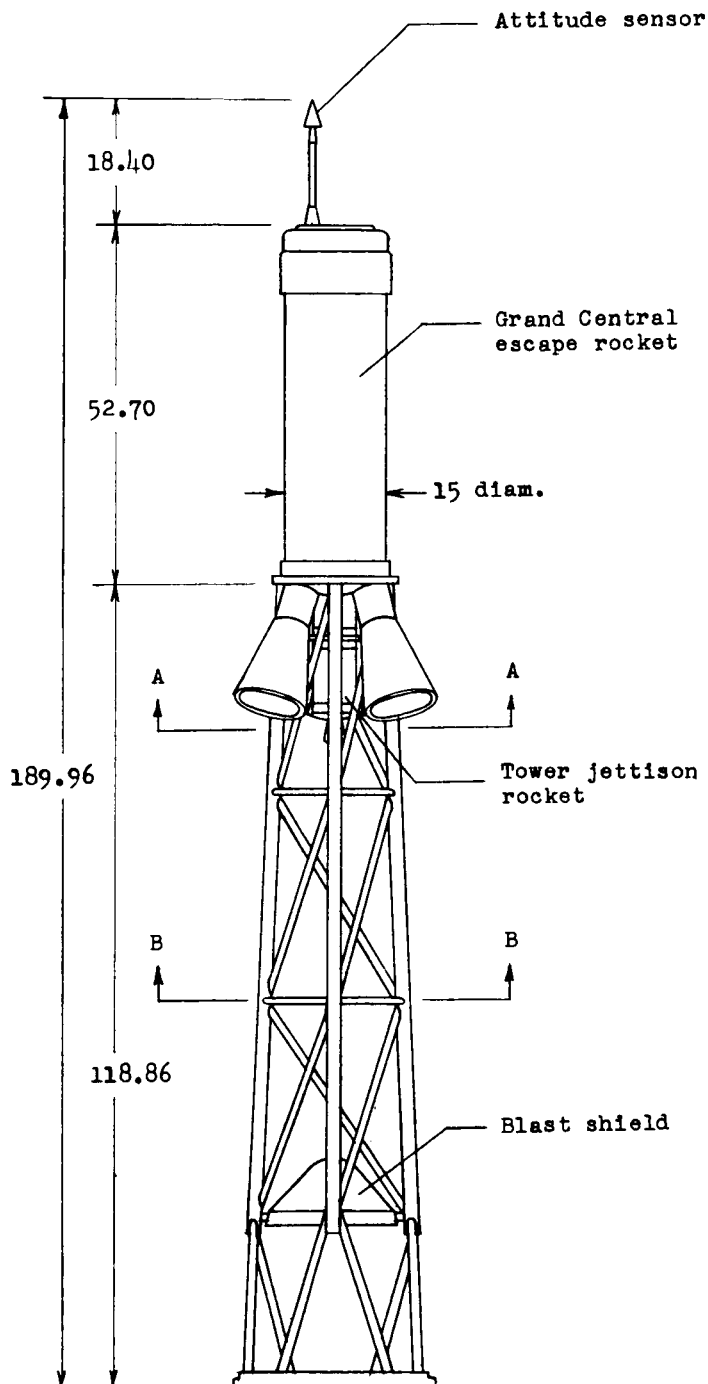


Figure 5.- Grand Central escape rocket and supporting tower.  
All dimensions are in inches.

~~CONFIDENTIAL~~

CONFIDENTIAL

37



B-60-30  
Figure 6.- Rhesus monkey being placed in the biopack insert.

I-1350

CONFIDENTIAL

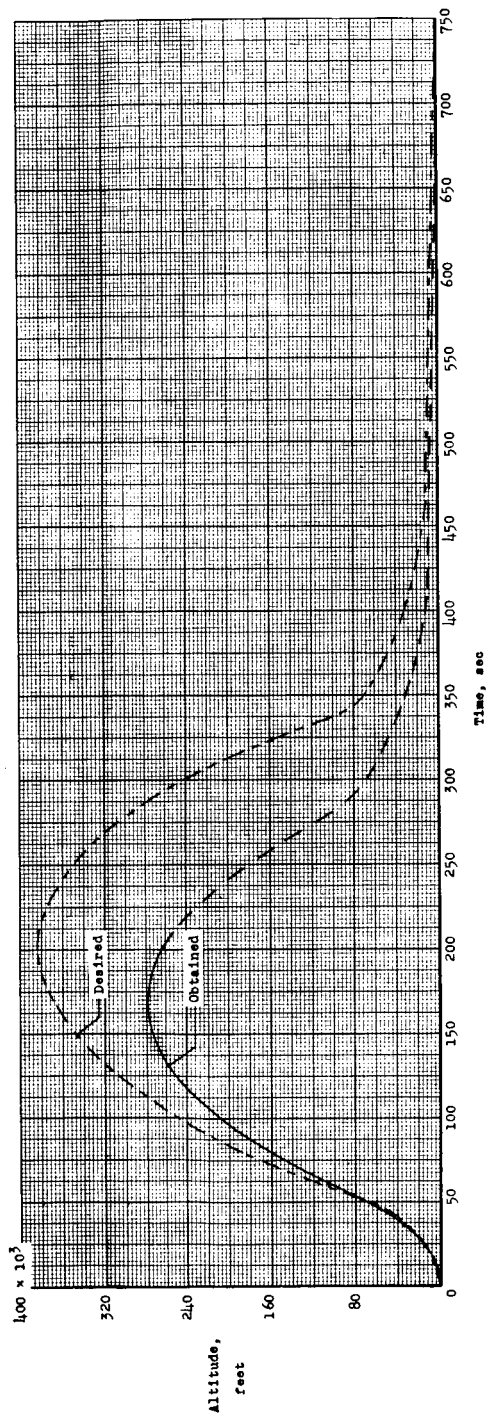


Figure 7.- Comparison of desired and obtained altitude time curves. Dashed portion of obtained altitude represents machine extrapolated data to drogue parachute deployment (373 seconds).

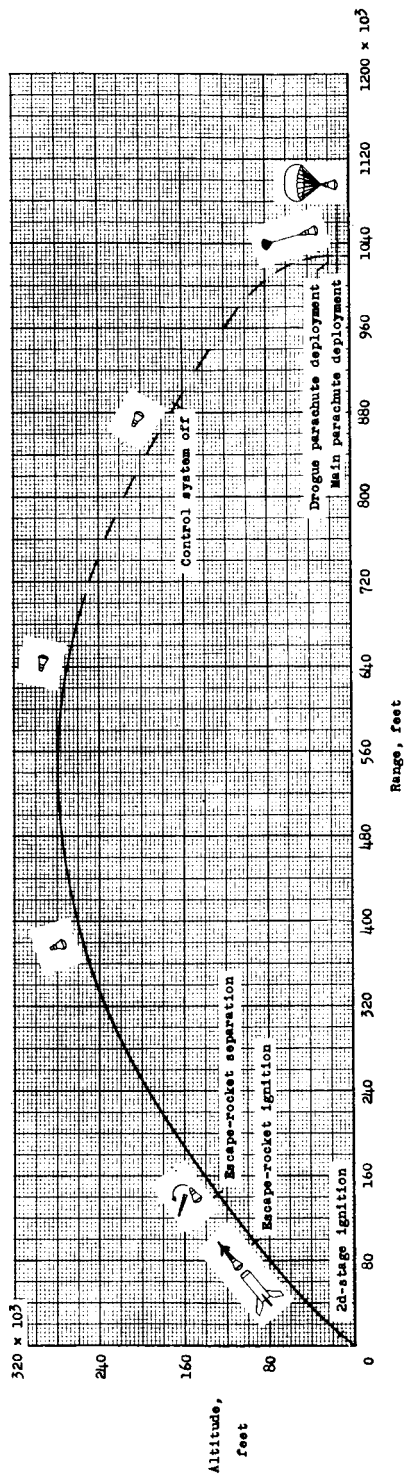


Figure 8.- Trajectory of the spacecraft. Dashed portion of the curve to drogue parachute deployment represents machine extrapolated data.

CONFIDENTIAL

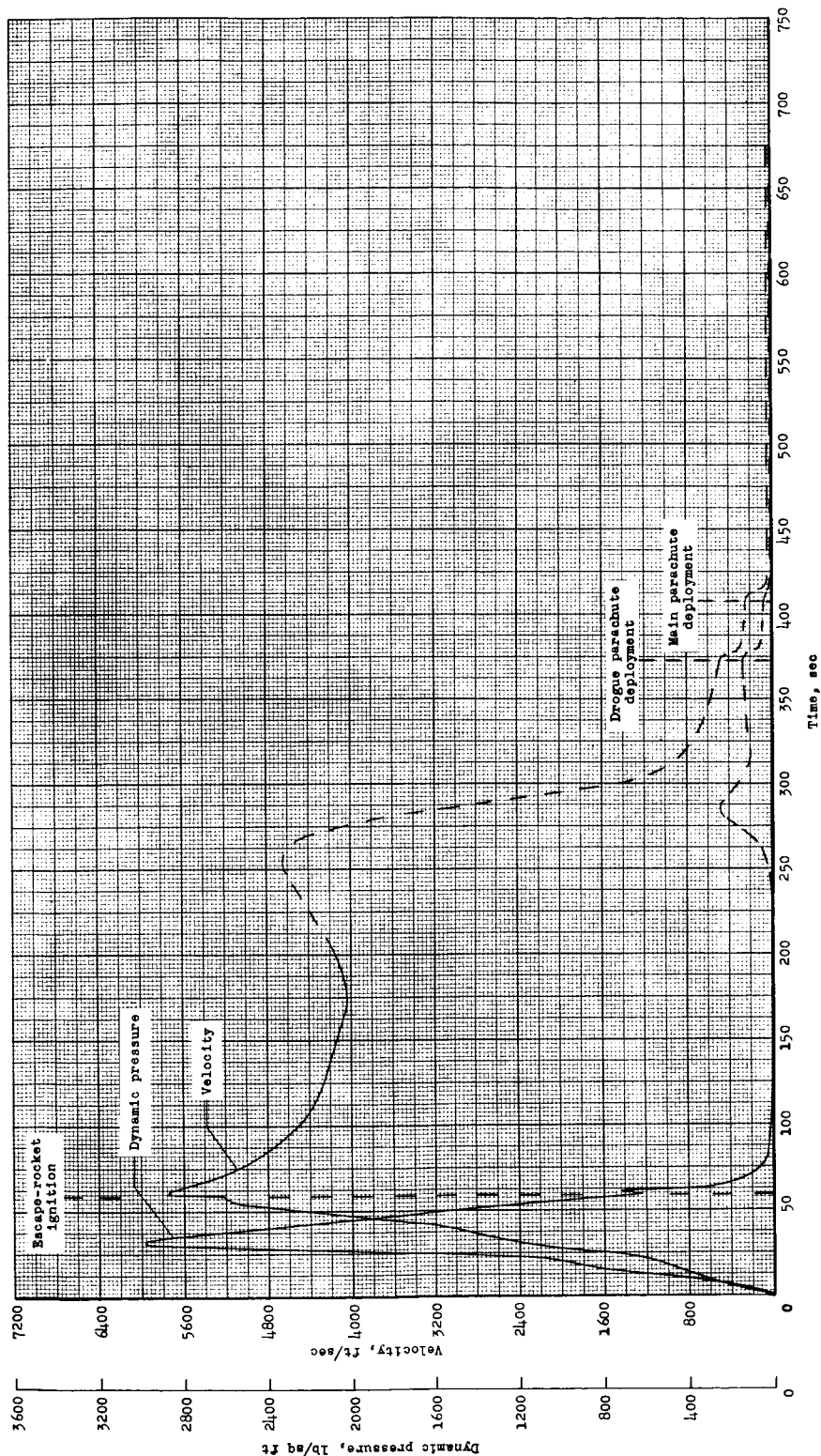


Figure 9.- Dynamic-pressure and velocity time histories. Dashed portions of curves to drogue parachute deployment represent machine extrapolated data.



CONFIDENTIAL

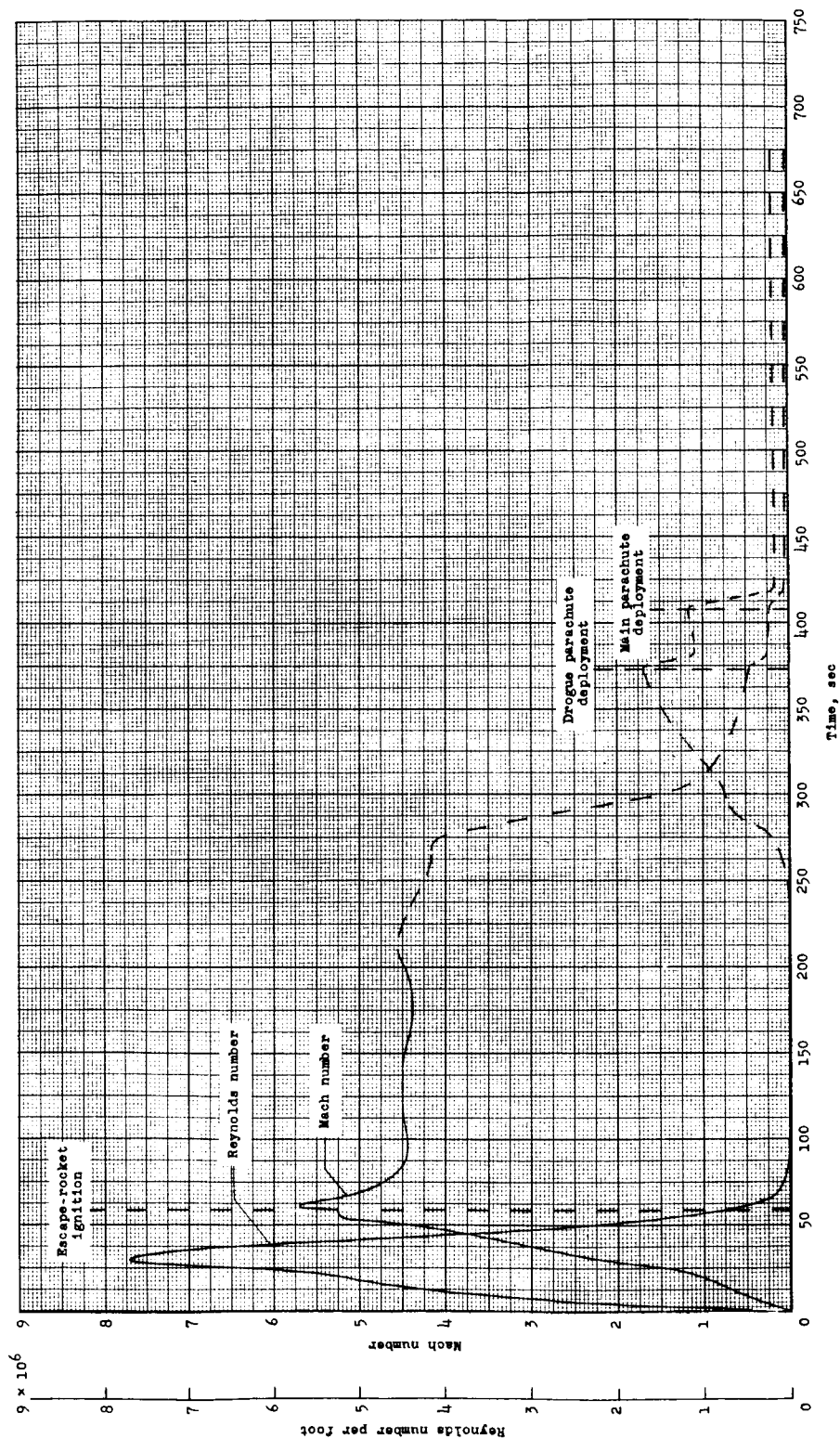
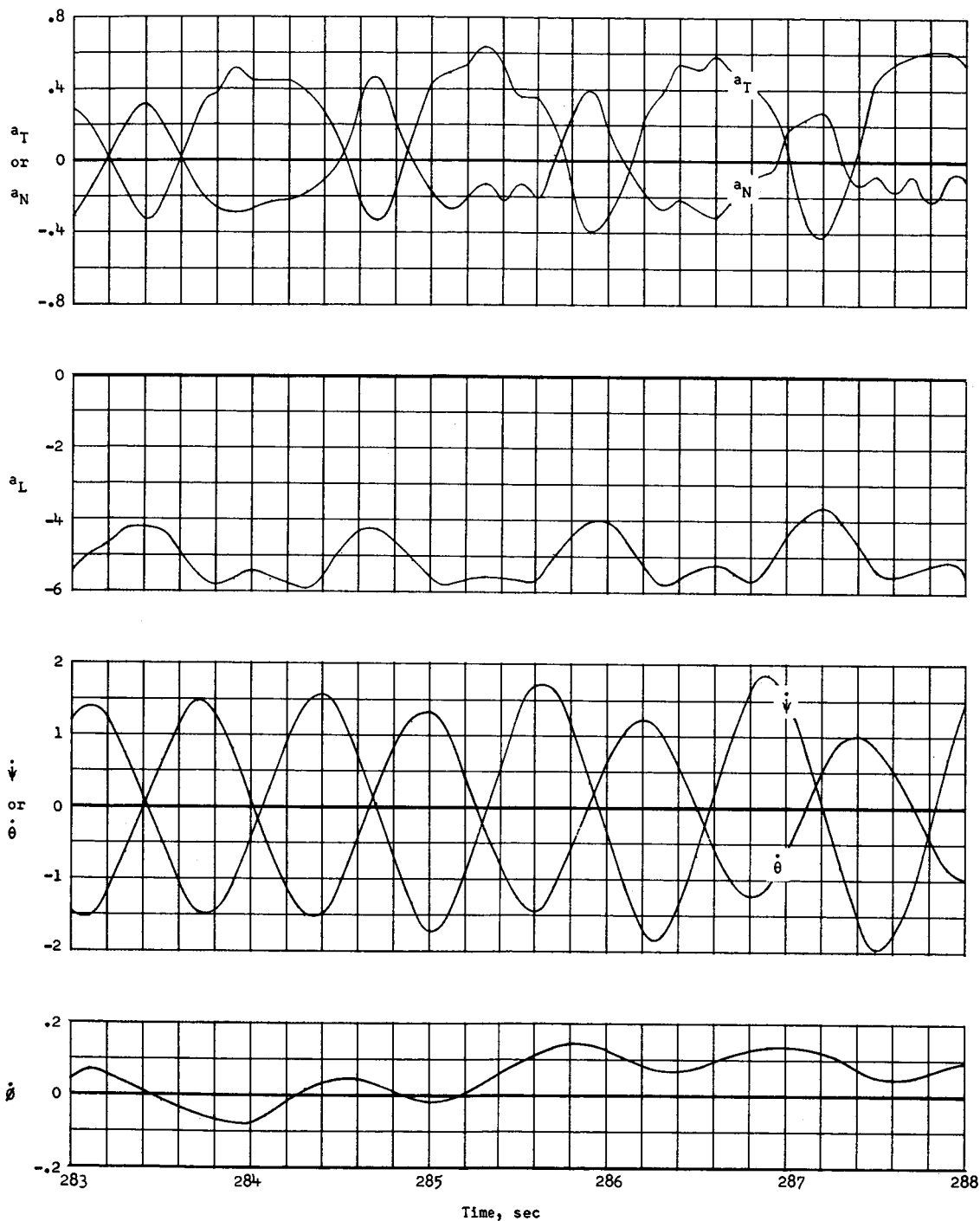


Figure 10.- Reynolds number and Mach number time histories. Dashed portions of curves to drogue parachute deployment represent machine extrapolated data.

CONFIDENTIAL

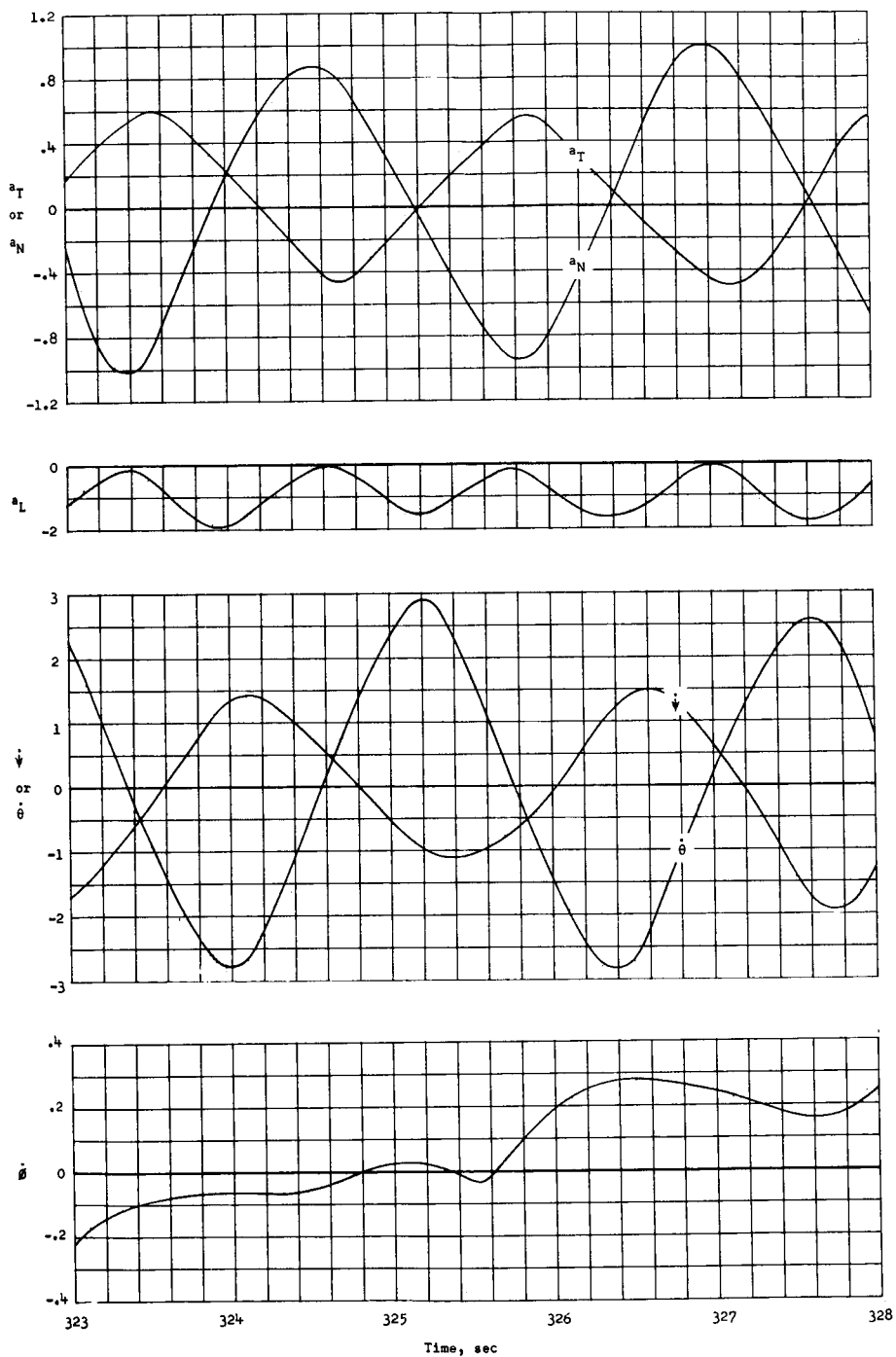
41



(a) Supersonic,  $M_{av} = 3.10$ .

Figure 11.- Sample time history of entry motion data.

CONFIDENTIAL



(b) Subsonic,  $M_{av} = 0.78$ .

Figure 11.- Concluded.

CONFIDENTIAL

CONFIDENTIAL

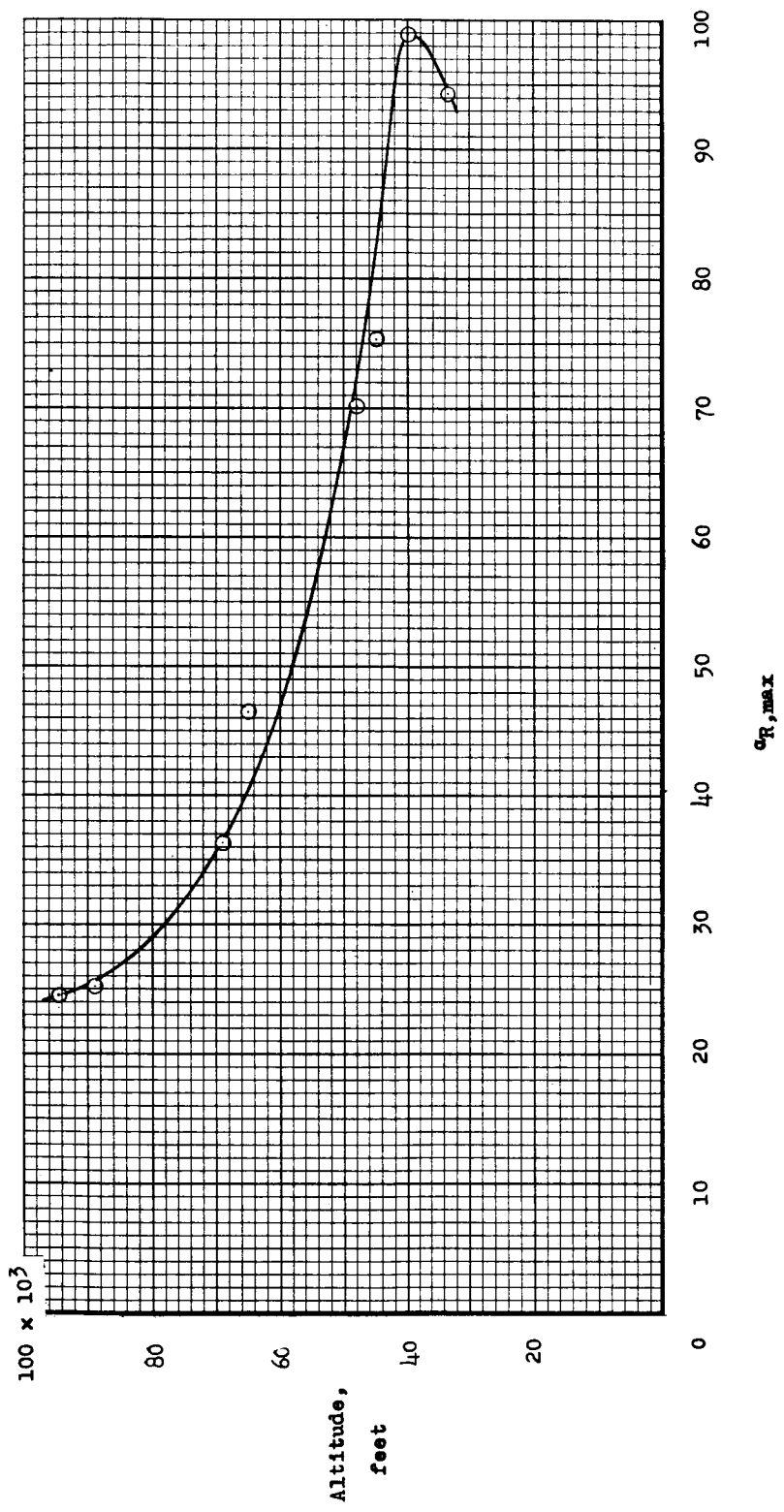


Figure 12.- Variation of maximum resultant angle of attack with altitude during entry.

CONFIDENTIAL

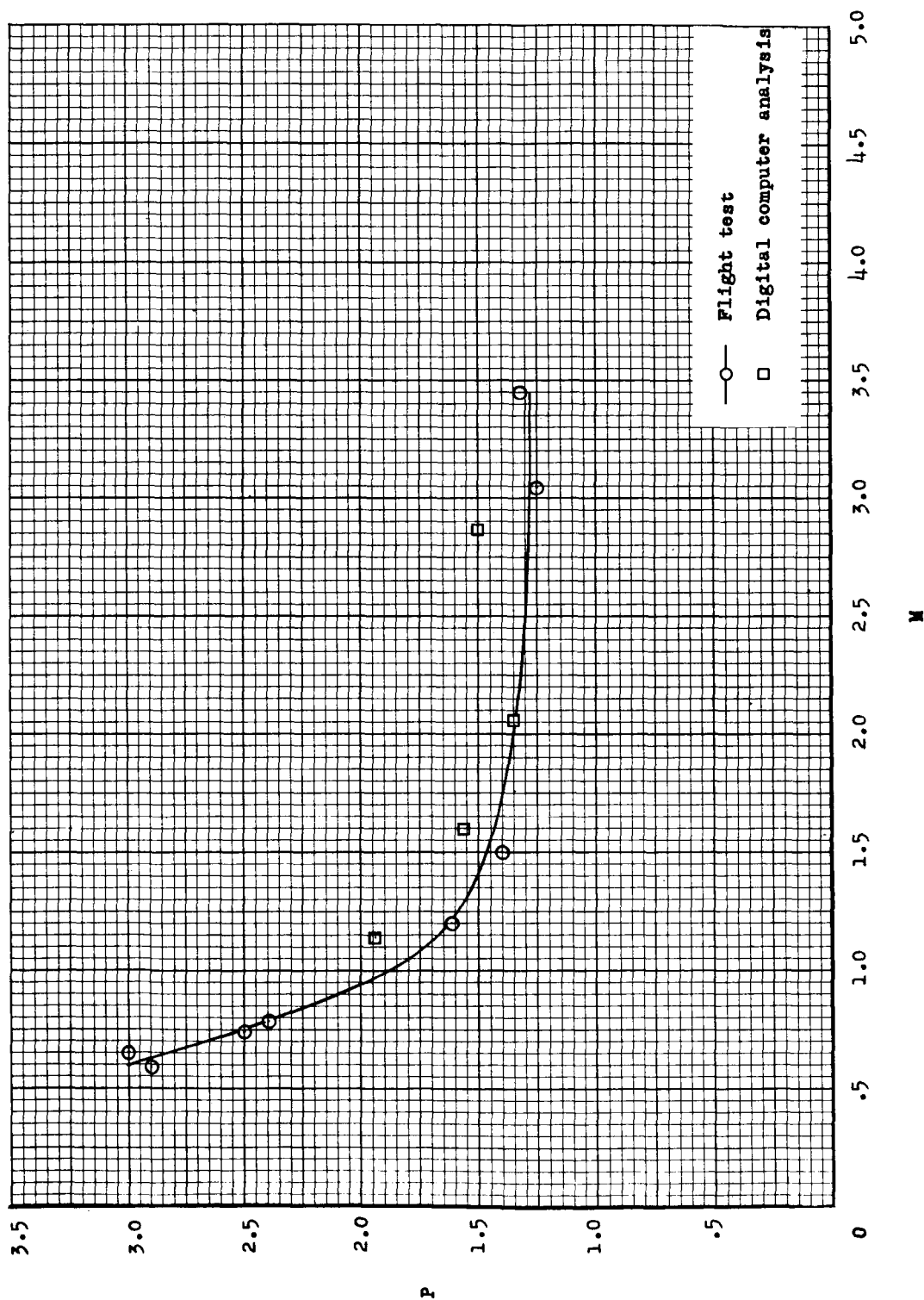


Figure 13.- Variation of period of oscillation with Mach number during entry.

CONFIDENTIAL

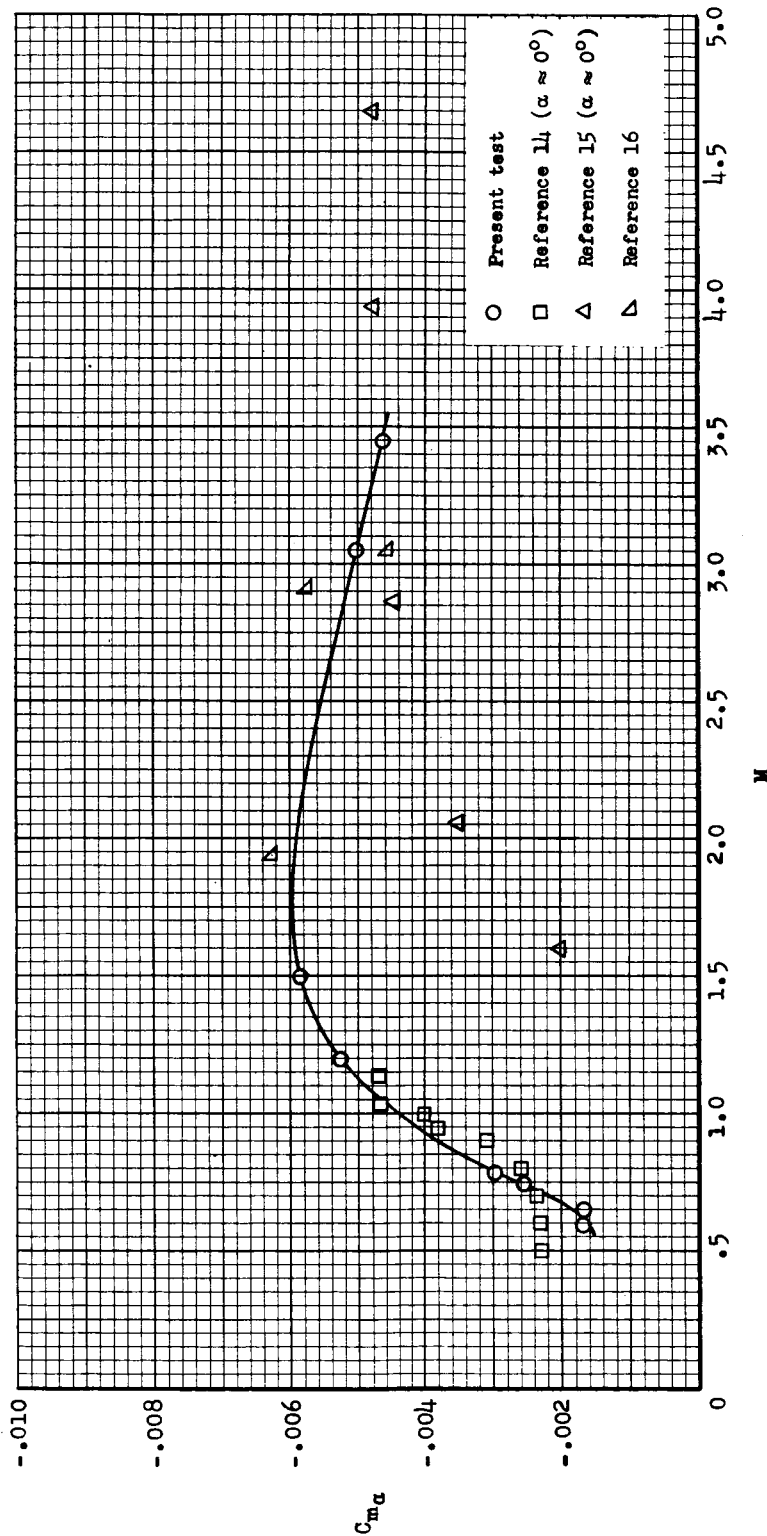


Figure 14.- Variation of static stability derivative with Mach number during entry.

CONFIDENTIAL

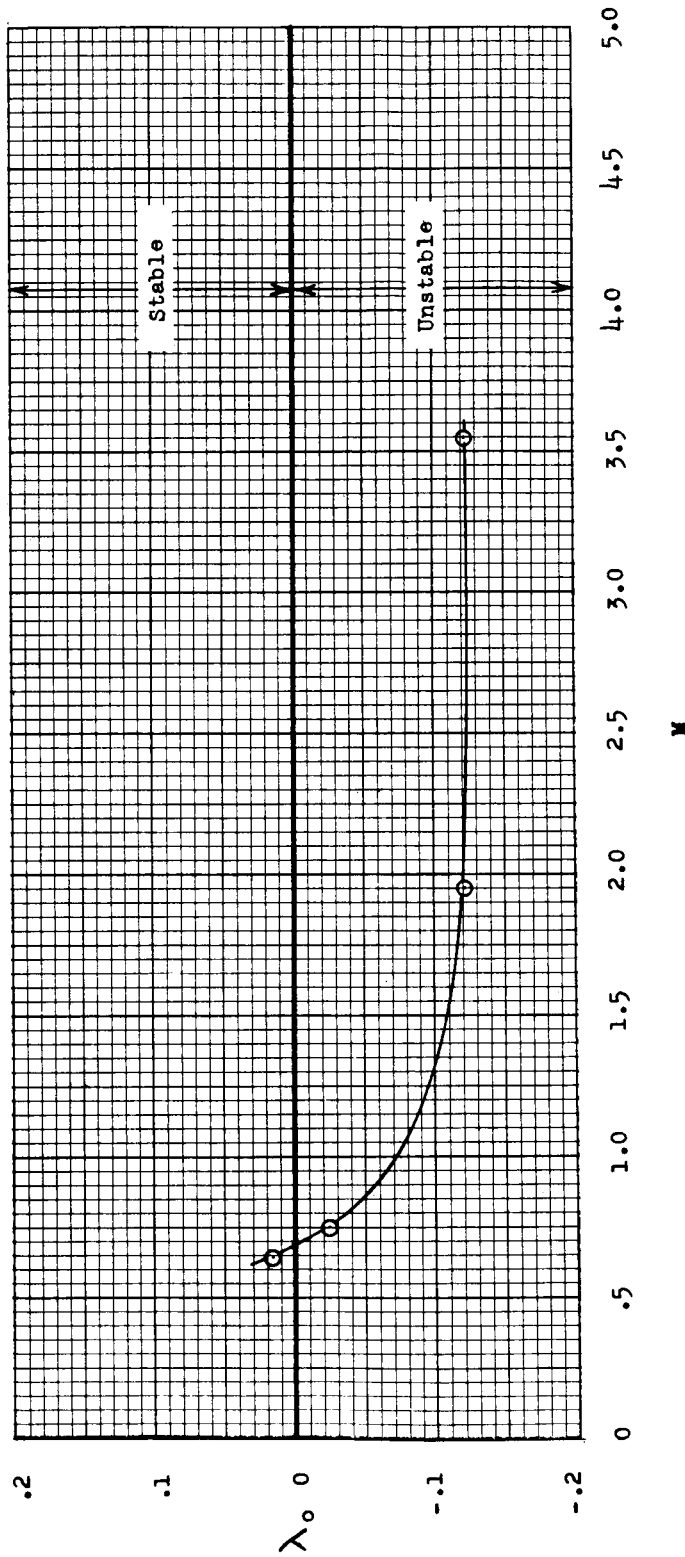


Figure 15.- Variation of exponential damping constant with Mach number during entry.

CONFIDENTIAL

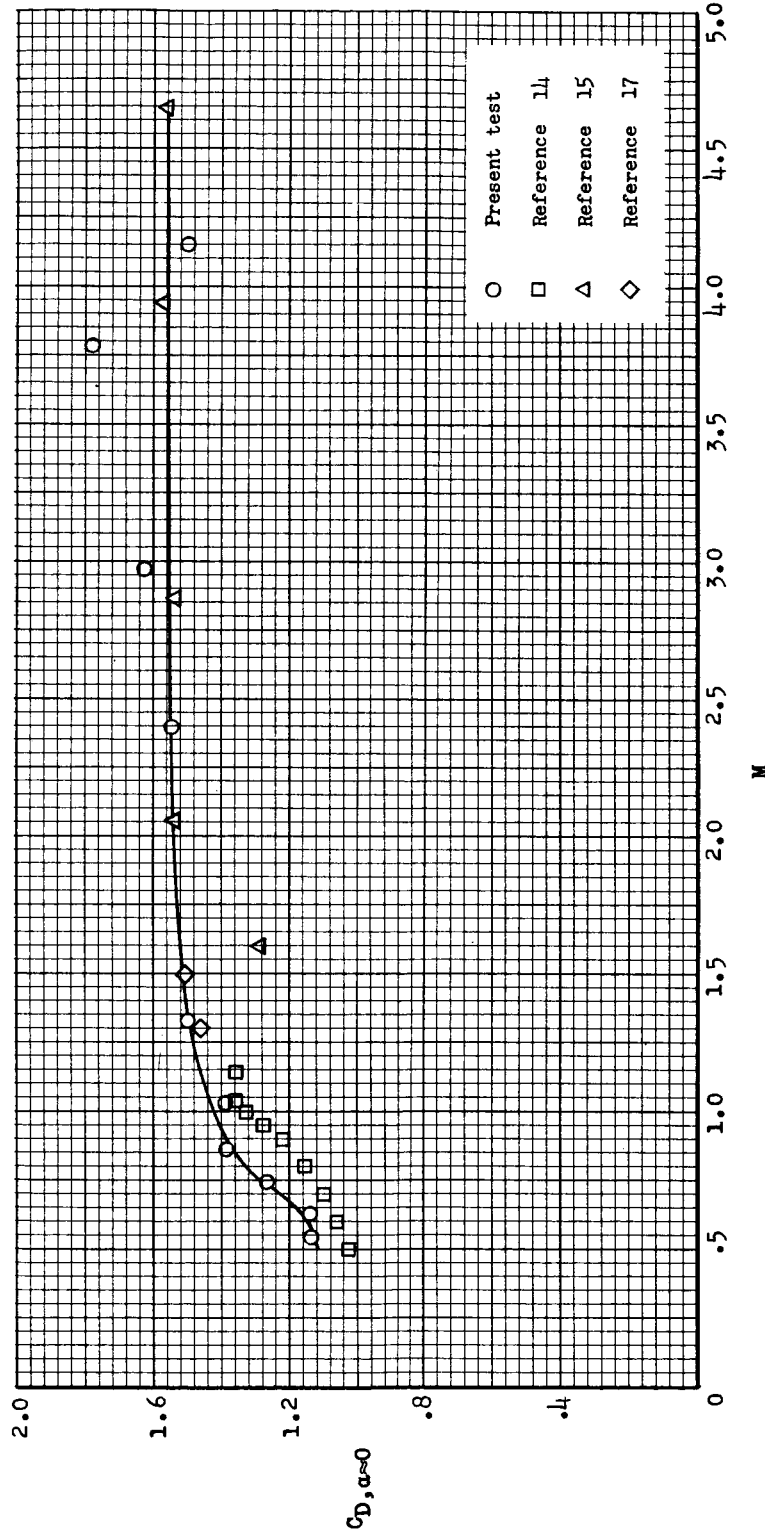


Figure 16.- Variation of spacecraft drag coefficient with Mach number during entry.



CONFIDENTIAL

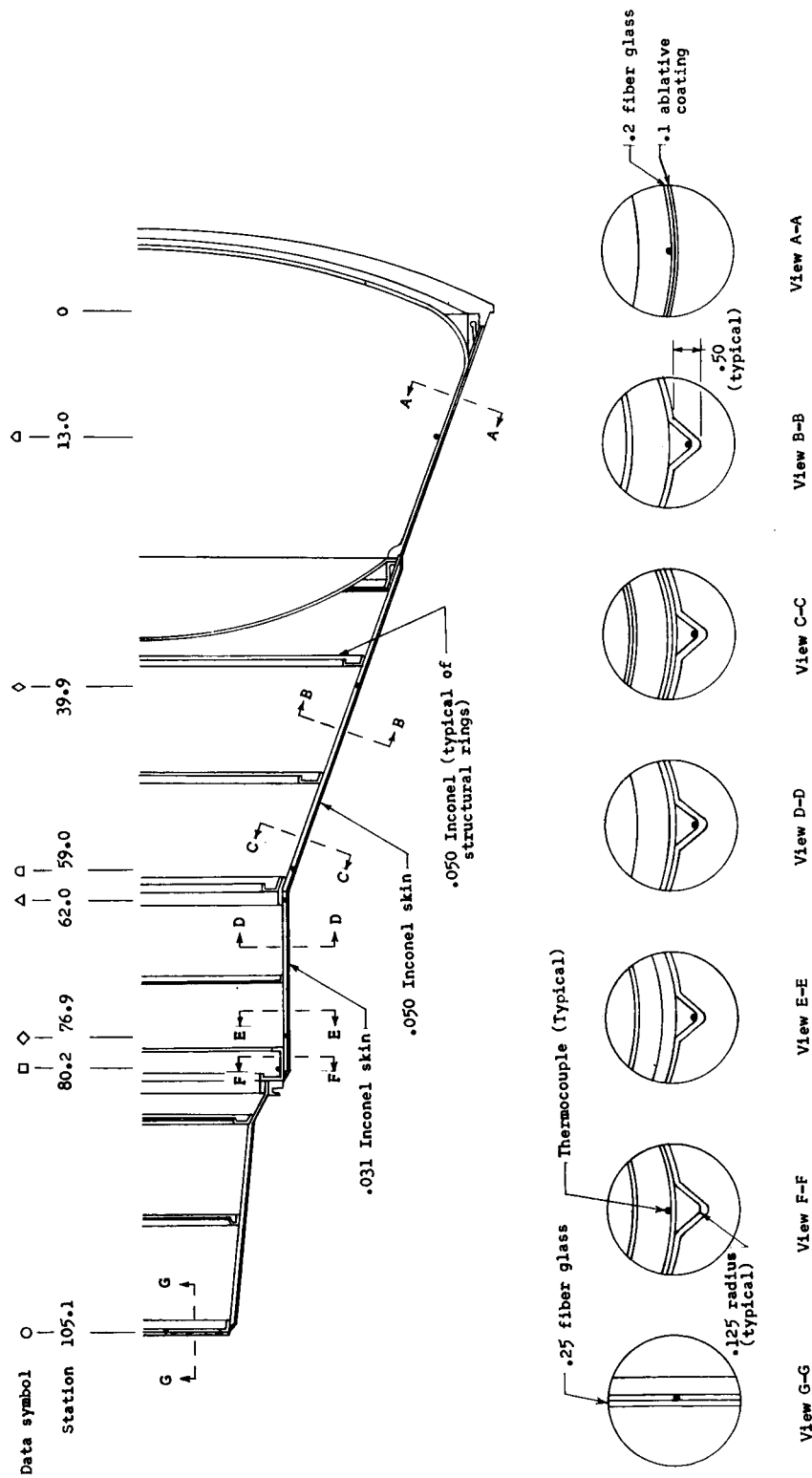


Figure 17.- Time histories of spacecraft inside-wall temperatures.

CONFIDENTIAL

49

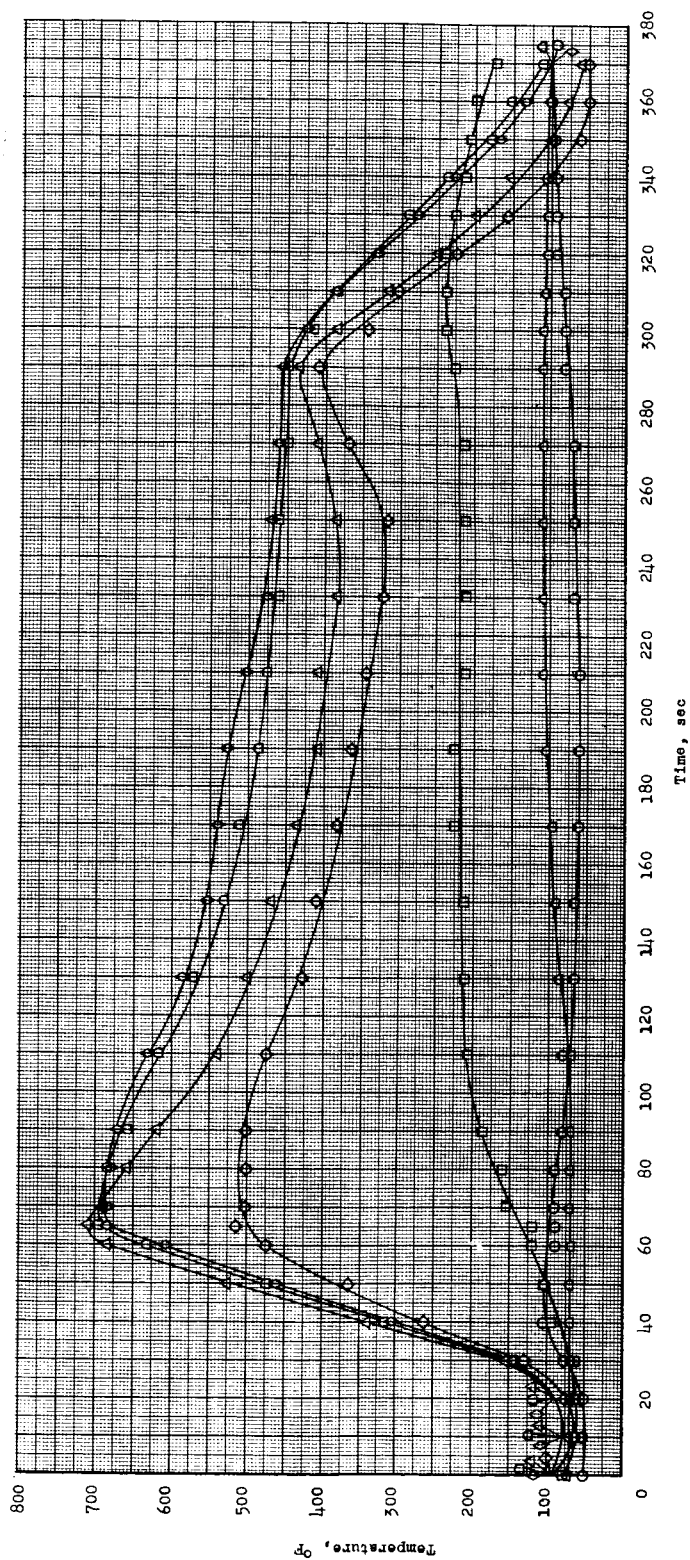


Figure 17.- Concluded.

CONFIDENTIAL

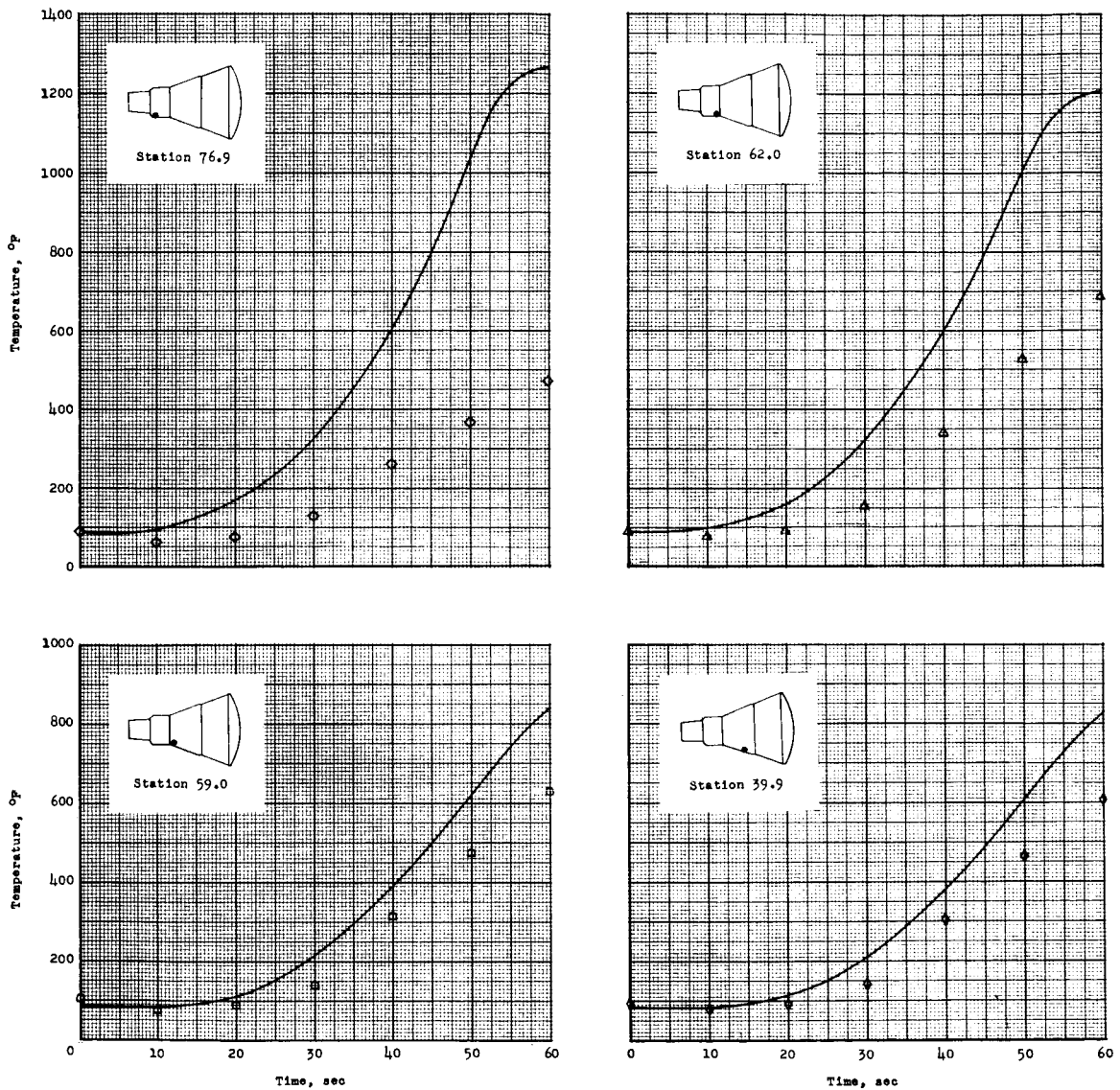


Figure 18.- Comparison of theoretical and measured temperatures for four stations on the spacecraft during the first 60 seconds of flight. Solid line indicates Van Driest's turbulent theory.

CONFIDENTIAL

51

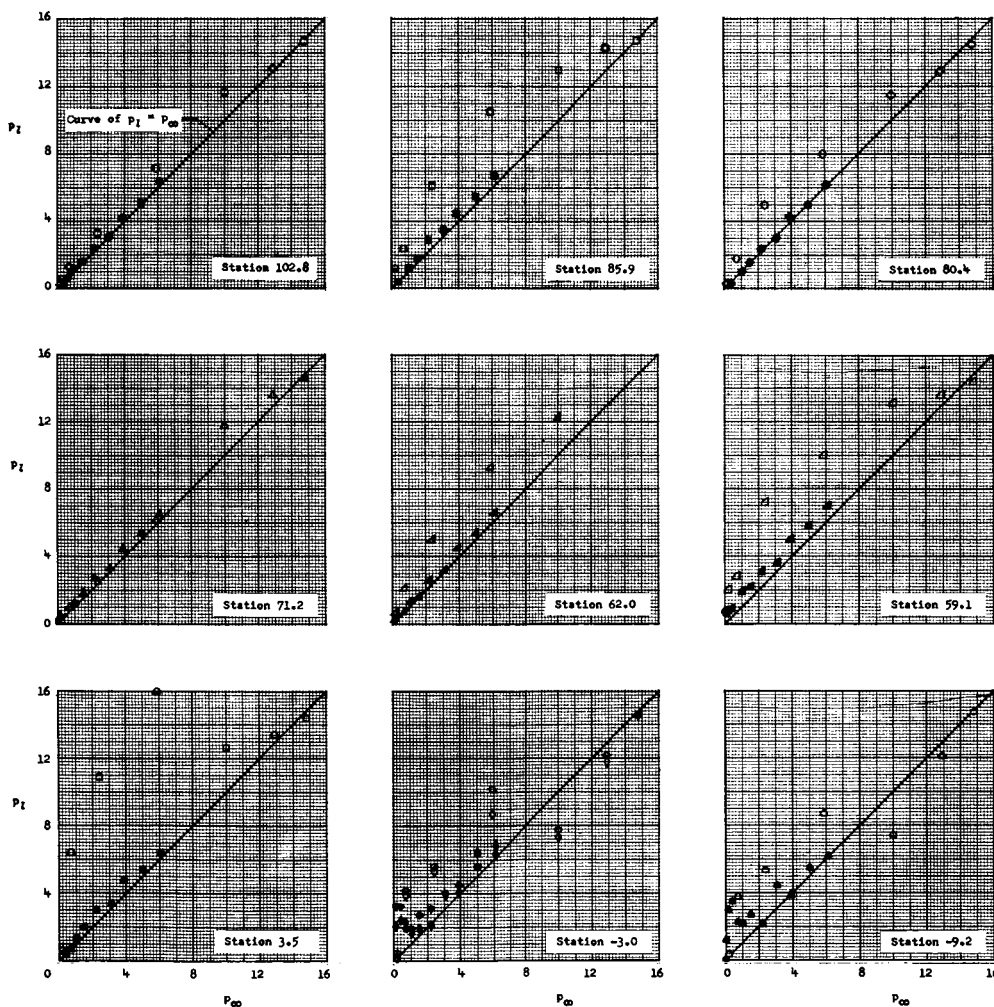
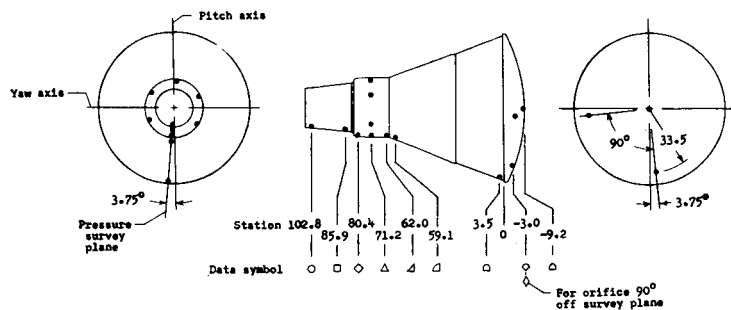


Figure 19.- Variation of local surface pressure with free-stream static pressure for several stations on the spacecraft. Open symbols represent data during ascending flight, and solid symbols represent data during descending flight.

CONFIDENTIAL

CONFIDENTIAL

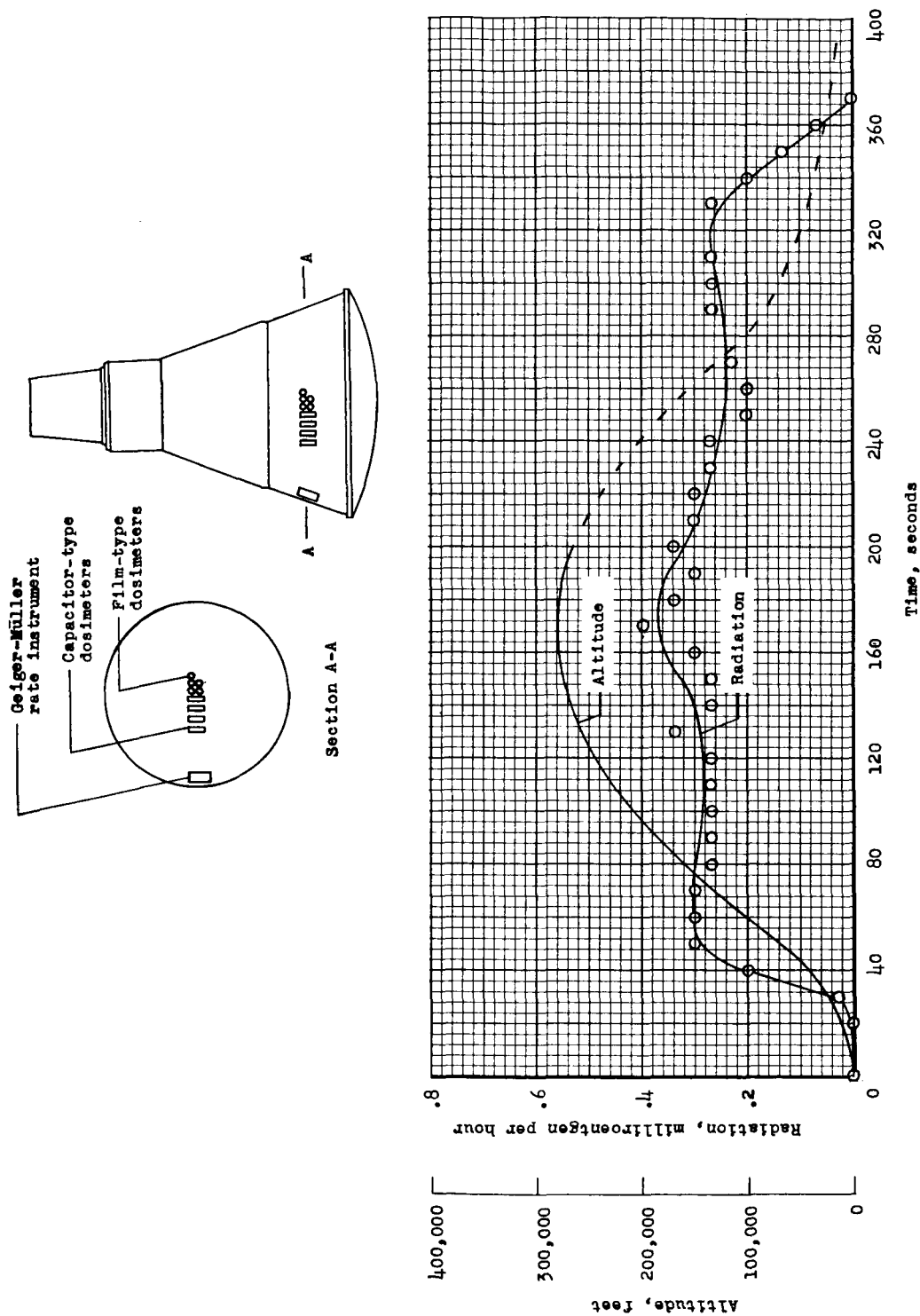


Figure 20.- Variation with time and altitude of the radiation measured by the Geiger-Müller rate instrument.

CONFIDENTIAL

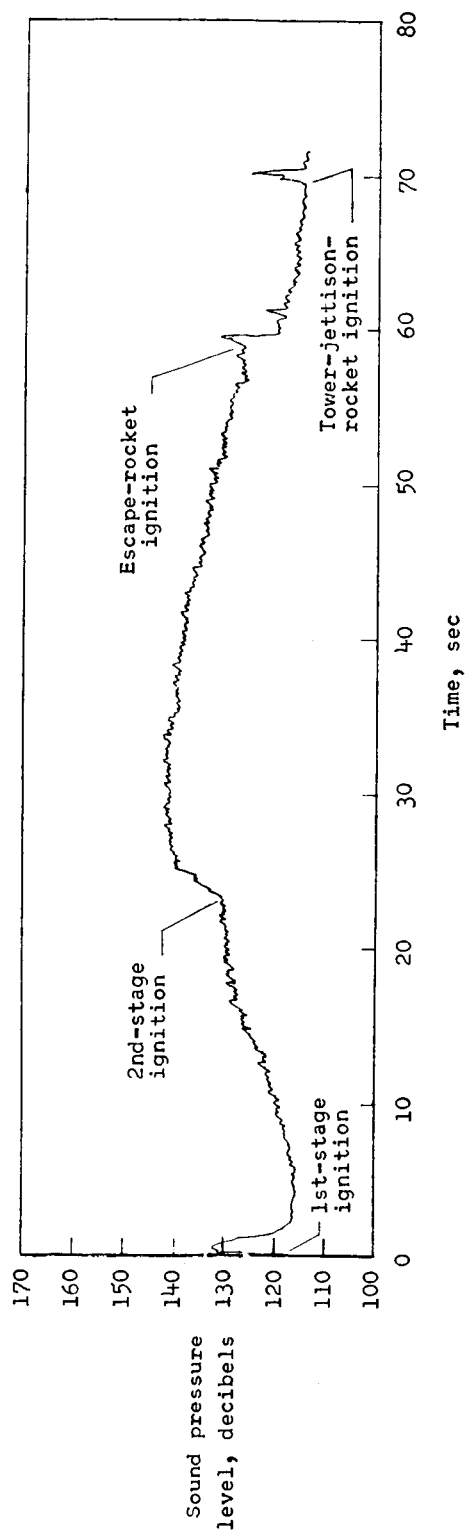


Figure 21.- Time history of noise inside the spacecraft measured during the flight.  
Reference level = 0.0002 dyne/cm<sup>2</sup>.